LA-UR-12-20464

Approved for public release; distribution is unlimited.

Title: A Report on MPDH Detectors for MaRIE, MWBS 1.2.2.3.1

Author(s):   Wang, Zhehui

Intended for: citeable document

NATIONAL LABORATORY

—— EST.1943 ——

A Report on MPDH Detectors for MaRIE, MWBS 1.2.2.3.1

Zhehui Wang, Cris W. Barnes[1], Stephen J. Greene,
Kris Kwiatkowski,[2] Sheng N. Luo and Christopher L. Morris

P-25, Subatomic Physics Group, Los Alamos National Laboratory
[1] P-DO, Physics Division Office, LANL
[2] P-23, Neutron Science and Technology Group, LANL

Summary

Coherent hard X-rays from FEL with energies in the range 10 - 100 keV, together with a 20-GeV electron beam and an 800-MeV proton beam, are being proposed for imaging of transient phenomena involving actinides in MPDH. Detector technology, like the light and charged particle sources and imaging systems, is a basic component of the facility. Compared with detections of energetic electrons and protons, detection of hard X-rays is more involved because of the need for photoelectric conversion.

The requirements of MPDH X-ray imaging system can be summarized as follows. Image frame time or gating (strobe) time is about one ps or shorter. Frame time is the time of signal integration for each frame of image. Time resolution (inter-frame time) is about three hundred ps or better. The total number of frames can be more than three thousands for a continuous movie that lasts for one microsec per event. The sample thickness is limited to about 100 μm for Pu-like high-Z samples due to X-ray attenuation. Thicker samples have to use charged particles, and in particular proton beams (see below). The spatial resolution is on the order 100 nm or less. The state-of-the art in resolution of X-ray imaging is less than 10 nm. The dynamic range of the detector covers single photon counting to about one million photons per pixel. Combined background and electronic noise therefore must be essentially about one electron or less in order to resolve individual photons. The detection efficiency needs to exceed 50% for 50 keV X-ray photons.

Correspondingly, the MPDH X-ray imaging cameras need to meet the following specifications. One ps gating (strobe) time could be achieved through the proposed sub-ps XFEL pulses. The fastest scintillators can respond within about 30 ps. Although the overall system response is about 1 ns or longer. The fastest semiconductors can, in principle, achieve similar response time as the fastest scintillators, depending on the detector size, operating temperature and wavelength of the X-ray photons. X-ray detection and signal recording must happen within 300 ps. Such a rapid signal recording may require in-pixel analog storage to eliminate the dead time due to signal transmission. Acquiring more

than three frames within 1 ns, or a frame rate above 3 billion frame per second for at least a microsecond, has not been demonstrated before. For Fraunhofer diffractive imaging, the detector voxel (For high detection efficiencies at 50 keV, the thickness of a conventional 'pixel' is now comparable to the other two dimensions, therefore 'voxel' is more appropriate) size is about the size of the sample, or as large as a few hundred μm for MPDH. The overall detector size is about one thousand times the pixel size per dimension, determined by the ratio of the sample size to spatial resolution. A dynamic range of $1:10^6$ requires at least 20 bits of recording depth. In short, although the basic mechanisms on how to detect hard X-rays are well understood and various aspects of detector specifications can be met using some existing technologies, the overall technological challenges to meet all of the MPDH requirements in a single detector (camera) are unprecedented and need further development.

Charged particle-based radiography and tomography methods can share the detector technology with X-ray methods. X-ray imaging methods provide a bottom-up tool to MPDH. Their main advantage is very fine spatial resolution (~ a few nm). They are however limited to very thin sample sizes (~ mm for low-Z samples and sub-mm for high-Z samples) due to attenuation of X-rays. A second limitation is the large sample-to-detector distance if Fraunhofer diffraction has to be used. The 20 GeV electron beam and 800 MeV pRad and tomography provide a top-down tool to MPDH and can examine meter-scale objects. Compared with electron methods, proton methods are less sensitive to multiple scattering and more mature. Proposal to extend the spatial resolutions of proton tomography to 10 μm or less exists. A limitation of the charged particle methods is their lower peak particle intensities than the brightest X-ray sources.

A dedicated research and development program is recommended to address three main challenges.

- The ps challenge. High efficiency (>50%) X-ray detection and recording needs to finish with a few hundred ps. There is an on-going pRad effort on a second-generation fast (50 ns) multi-frame imager. It is expected that at 10 keV X-ray energy, the existing 100 µm thick Si sensor can be used as a fast high-efficiency (above 50%) direct-detection imager. Later on, new generations of detectors based on high electron mobility and higher Z materials, such as GaAs or InSb, can be developed.

- The GHz challenge. Imaging frame rates needs to be at a few GHz for fast X-ray movies.

- The TB challenge. MPDH data rate is 1.2×10^{19} byte of data per second $= 3 \times 10^9$ (frame rate) x 10^6 (number of pixels) x 10^6 (dynamic range)/ 256 (8 bit per byte) for at least 1 μs (or ~ 10 TB per event). Significant involvements from micro-fabrication industry (ASIC technologies), academia, and possibly other DoE laboratories may be necessary to address the challenge.

Table of Contents

1. Introduction

Matter-Radiation Interactions in Extremes (MaRIE) addresses the micron frontier of materials, which bridges understanding on the atomic scale and performances on a bulk scale.[1] As a key component of MaRIE, the central focus of the multi-probe diagnostic hall (MPDH) is on dynamic compression experiments.[2] Various driver systems, such as gas guns, powder guns, lasers, high explosives, and electromagnetic compression, will be used directly or indirectly to drive shock waves through materials for 10's of ns to a few μs. A suite of XFEL (10 to 50 keV, tunable), electron (20 GeV) and proton beams (~1 GeV), combined with spectroscopic (for temperature), velocimetric, and pyrometric diagnostics, will map material evolution in real time and reveal materials physics and chemistry at smaller length scales, in multiple dimensions, and for a large dynamic range in time (from ps up to μs). Detector technology, like the light and particles sources and the imaging system, is another basic building block of the facility. This report analyzes the existing detector technologies for their relevance to MDPH missions, identifies gaps and addresses R&D needs on detector development.

MPDH functional requirements

Pressures in the universe span more than 60 orders of magnitude, from 10^{-32} times the sea-level atmospheric pressure in intergalactic space to 10^{31} times the atmospheric pressure in the center of a neutron star.[3] In comparison, the driver systems in MPDH can potentially deliver pressures up to a few hundred GPa (4 - 200 GPa, to be specific), close to the pressure in the core of the Earth (363 GPa). Shock-wave methods can produce much higher pressures than static methods using, for example, diamond anvil cell, although sample heating due to strong shock-waves may limit the ultimate compression to a few hundred TPa.[4] It is remarkable that pressure, internal energy and compression (volume) are completely determined by the shock velocity (u_s), and the velocity of compressed material behind the shock front, normally known as particle velocity (u_p).[5] For the proposed MPDH drivers, the shock velocities would be about 10 km/s. For an iron projectile, the impact pressure at 10 km/s is up to ~ $0.5\rho v^2$, or about 400 GPa. The corresponding particle velocity would be less, on the order of a few km/s. High power ultra-short pulse lasers may produce higher pressure than projectiles, but the spot sizes are smaller and duration can be much less than a 1 ns, too fast for heavy ions to respond in time. Since material physics and

---

[1] Experimental Physical Sciences VISTAS, LALP-10-059 (Fall 2010).

[2] D. Robbins et al, *MaRIE MPDH Sub-committee on Shock Drive System Evaluation* (Aug. 2011).

[3] R. J. Hemley and N. W. Ashcroft, The revealing role of pressure in the condensed matter sciences, *Phys. Today* **51** (1998) 26; R. J. Hemley, A pressing matter, *Phys. World,* August (2006) 26.

[4] R. F. Trunin, *Shock compression of condensed materials*, (Cambridge University Press), p.4.

[5] Rice, McQueen, and Walsh, in *Solid State Physics, vol.* **6** (1958) 1-63; J. N. Johnson and R. Cheret, *Classical papers in shock compression science,* (Springer, 1998) p. 133 and p.161; C. E. Morris, Shock-wave equation-of-state studies at Los Alamos, *Shock Wave* **1**, (1991) 213.

chemistry depend on energy input from the shock front, the time scales of evolution are dictated by the shock propagation time through samples.
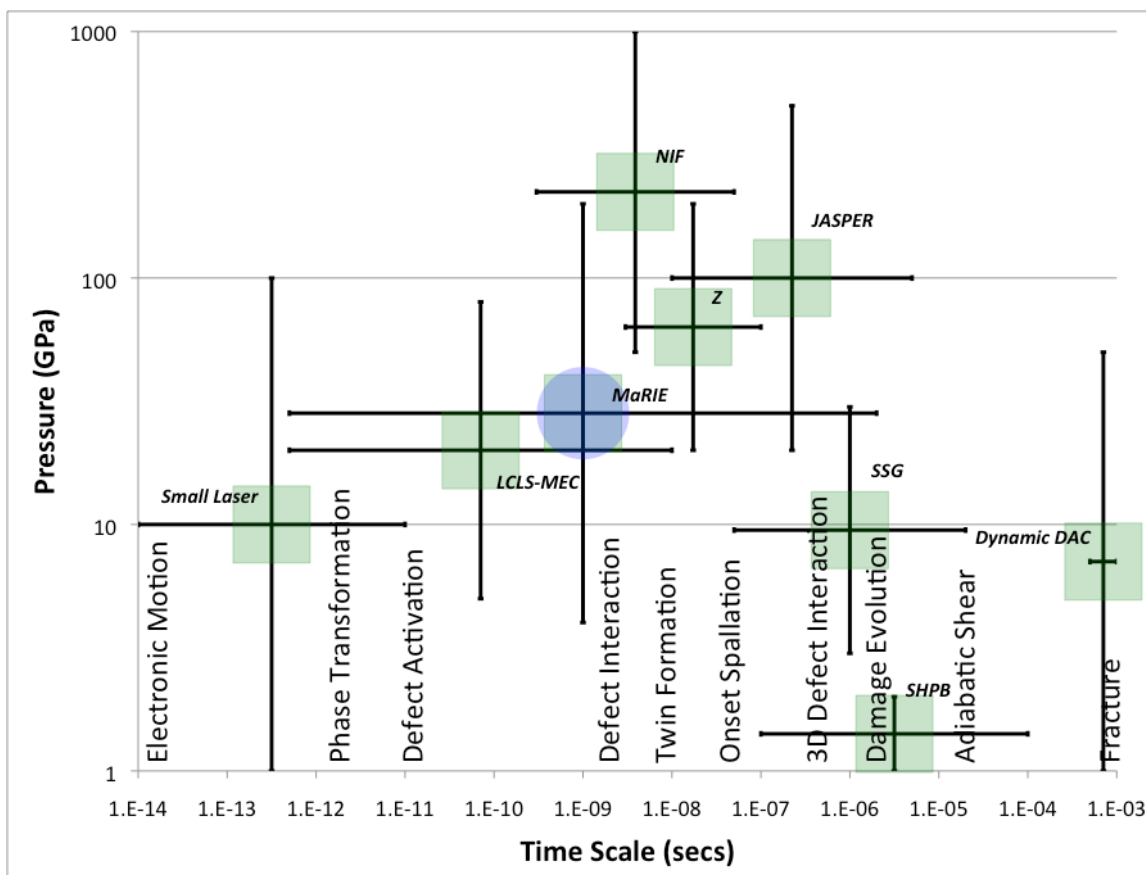
Figure 1. Time scales of interest to MPDH.[6]

A minimum of several grain thicknesses in all directions is needed for an accurate representation of the bulk.[6] Because of the strong Z-dependence of the X-ray transmission through matter, the allowable thickness varies significantly from low-Z to high-Z materials for similar X-ray transmission. For Pu with a grain size of 10 μm, ten grains corresponds to a thickness of 100 micron. Penetration of the thickness requires at least 50 keV (0.025 nm in wavelength) X-ray photons. The corresponding transmission direction thickness for aluminum is about 2.0 mm.

The materials physics and chemistry of interest extends from sub-ps to tens of μs in time.[6] For high-pressure shock fronts moving at 10 km/s (10 μm/ns) with no blurring at 1 micron resolution gives a maximum radiography (density) pulse length of 100 ps duration. Chemical bonds break, form, or geometrically change

---

[6] C. Bronkhorst, Carl Greeff, George Gray III et al., *Microstructure based heterogeneity Evolution leading to material phase transformation and damage/failure events, MaRIE report (2010).*

with awesome rapidity.[7] Whether in isolation or in any other phase, this ultrafast transformation is a dynamic process involving the mechanical motion of electrons and atomic nuclei. The speed of atomic motion is ~1 km/s (thermal motion at room temperature) and, hence, to record atomic-scale dynamics over a distance of an angstrom (the characteristic distance between neighboring atoms in a solid/liquid), the average time required is ~100 femtoseconds (fs). The electron motion and electron-to-electron interaction, would be about 40 times faster, or a few fs. Phase transformations, or re-arrangements of atomic positions, are predicted to occur in a few ps. Further physical and chemical processes are summarized in Figure 1.

Experimentally, the time sequence to record an event can be broken down as follows, Figure 2. The ideal "gating time" or "frame time" of imaging measurements is needed to be sub-ps. Shock will traverse a single grain in one to several nanoseconds; if a few individual measurements are desired during shock transit across a grain the "time resolution" between measurements needs to be as little as about one-third of a nanosecond or 3 GHz. An assumption (see above) is to have up to 0.5-μs transit time across the sample. A single event (movie) is consists of at least 20 and up to 1500 individual imaging frames; a static image of the unperturbed sample is also needed. The synchronization of the shock front with the probes should be less than the transit time across a grain which could be as little as one nanosecond.
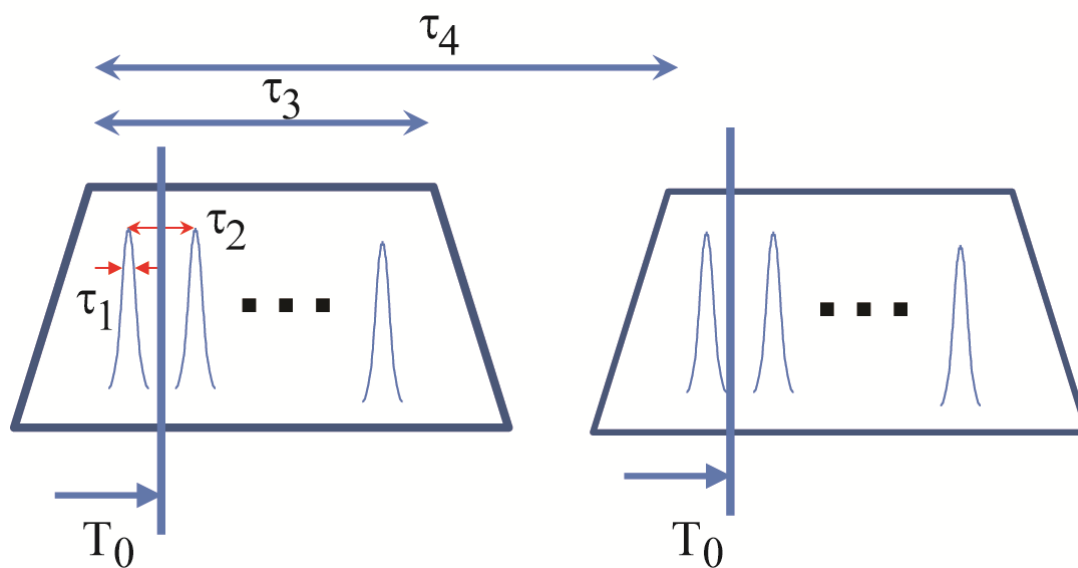
Figure 2. A summary of experimental time sequence. τ_1, also known as gating or frame time, corresponds to the X-ray pulse length, each pulse generates one frame of image. τ_2, also known as the time resolution, corresponds to pulse-to-pulse separation. τ_3 defines the duration of an event. The sequence of pulses forms so-called single macro-pulse. τ_4 defines the repetition time between events, $1/\tau_4$ defines the repetition rate of macropulses. T_0 is the time when a shock arrives at a sample. Prior to T_0, one obtains static or unperturbed images of a sample. At least one static image is needed for comparison with subsequent images.

[7] A. H. Zewail, *Femtochemistry, Past, present and future,* Pure Appl. Chem. **72**, (2000) 2219.

Spatial resolution is determined by feature sizes of interest at the object location. Such features may include grain size, grain-boundary thickness, shock layer thickness, and products of characteristic velocities with certain time duration. Spatial resolution, as well as temporal resolution, is also affected by imaging methods (magnification) and detectors. The goal of spatial resolution of three-dimensional X-ray measurements is at 1.0 micron, with a beam spot size up to 100 micron in diameter. The ratio of the field-of-view to spatial resolution determines the detector size.

X-ray imaging will be supplemented by a 20 GeV electron beam and the existing 800 MeV proton beam for radiography in the transverse dimensions to the direction of X-ray beam, where the sample thicknesses prevent X-ray from transmitting through samples. The 20 GeV electron beam can potentially deliver 1.0 micron or finer spatial resolution. Proton radiography has about 100 micron spatial resolution at the moment. Both of them will be used to map density profiles and their time evolution. Current pRad at LANSCE provides a 50-nsec frame time and about 20 frames per microsecond. It should be mentioned that neither charged beam is harvested for its phase information or spin information. If the revolution of X-ray imaging from radiography to imaging through phase information is any guide, a coherent charged particle or a spin-polarized beam is worthy of further investigation for radiography or imaging, in parallel with the detector development. Coherent electron sources at low energies (< 1 MeV) and their applications have made significant progress.[8] A key challenge is to develop a coherent beam in the GeV range. Spin polarized proton or electron beams have been developed and studied more extensively under the context of High-Energy Particle (HEP) physics.

Detector requirements

Here, detector requirement discussion is based on far-field coherent diffraction imaging (CDI), or coherent imaging based on Fraunhofer diffraction, without using a lens. The following set of equations determines the image size and resolution at the detector location.[9]

Detector to sample distance (z):

$$z = \frac{1}{N_F} \frac{O^2 a^2}{\lambda} \, , \tag{1}$$

where a is the size of the sample, and λ the X-ray wavelength. The oversampling ratio O is explained below. Fraunhofer diffraction is characterized by a small

---

[8] J. M. Zuo et al, *Science* **300** (2003) 1419; A. Tonomura, *The quantum world unveiled by electron waves,* (World Scientific, Singapore, 1998); F. Hasselbach, *Progress in electron- and ion-interferometry,* Rep. Prog. Phys. **73** (2010) 016101;

[9] J. Miao, T. Ishikawa, E. H. Anderson, K. O. Hodgson, *Phase retrieval of diffraction patterns from noncrystalline samples using the oversampling method,* Phys. Rev. B **67** (2003) 174104.

Fresnel number $N_F \ll 1$. For practical purposes, one may choose $N_F \leq 1/2$.[10] For a sample size of a = 10 micron and an X-ray wavelength of 0.124 nm (10 keV), the Fraunhofer condition can be achieved at a distance greater than 3.2 m (For O=1.41). For a sample size of a =100 micron, the detector distance increases by a factor of 100, to about 320 m. For 50 keV X-rays (a wavelength of 0.025 nm), a sample size of 100 micron corresponds to a distance of 1600 m, which may not be practical. In other words, near-field imaging method may have to be used for 50 keV X-ray and large samples.
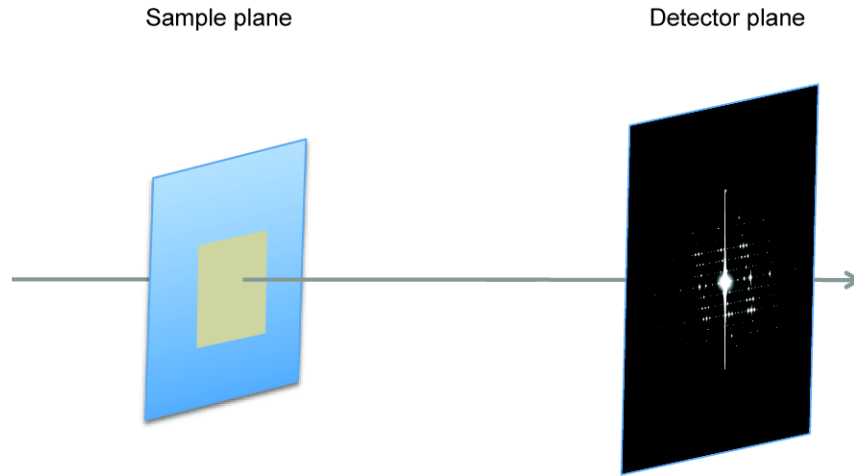
Figure 3. An imaging process is a form of information transfer. From the sample plane to the detector plane, the information content can not increase. Diffractive imaging sets the upper limit on the information transfer, normally described in terms of resolutions. The same arguments also apply to the source-sample information transfer in the sense that the source limits the bandwidth that can be transferred of the information about the sample.

It is useful to recognize that, in diffractive imaging, limitation in information transfer[11] is usually described in terms of resolutions. Using Rayleigh's resolution criterion, the spatial resolution (δ) on a plane perpendicular to the direction of illumination is given by[12]

$$\delta = \frac{1}{2}\frac{\lambda}{\sin\theta} \quad . \tag{2}$$

The above equation can be casted into different forms. If δ stands for the spatial resolution of the sample plane, θ is the smaller of two angles, angular extent of the detector or the maximum angle at which phase can be reliably assigned (determined by the bandwidth of the source). Assuming that the source coherence is not the limiting factor, then θ is determined by the detector size (L_D)

---

[10] Corresponding to a phase change across the sample of $\pi/2$ or less. See A. Lipson, S. G. Lipson, and H. Lipson, *Optical Physics (4th Ed.)* (Cambridge University Press, 2011) p. 203.

[11] Which is related to the uncertainty principle.

[12] K. A. Nugent, *Coherent methods in the X-ray sciences,* Advances in Physics, **59**:1, 1-99.

$$\sin\theta \sim \theta \sim \frac{L_D}{2z} \quad . \tag{3}$$

Combining Eqs. (1), (2) and (3), one has the overall detector size using a perfectly coherent source as

$$L_D = \frac{\lambda z}{\delta} = \frac{O^2 a^2}{N_F \delta}, \tag{4}$$

If δ is equal to the pixel size (l_p) on the detector plane, then θ in Eq. (2) is the angular extent of the sample, or an extended sample,

$$\sin\theta \sim \theta \sim \frac{Oa}{2z}, \tag{5}$$

From Eqs. (1), (2) and (5), one obtains

$$l_p = \frac{z\lambda}{Oa} = \frac{Oa}{N_F} \quad , \tag{6}$$

Finer pixel sizes (or 'pitches') do not improve the resolution and are unnecessary. Oversampling of a diffraction pattern is needed to recover the phase and thus the electron density information through inverse Fourier transform. Oversampling a diffraction pattern at a spacing finer than the Bragg peak frequency (also known as the Niquist frequency) corresponds to surrounding the sample with a zero-density region.[13] As shown in[9], $O \geq 2$ is sufficient. For an oversampling region of $Oa \sim 200~\mu m$, the pixel size can be about 400 μm with $N_F = 1/2$.

From Eqs. (4) and (6), both the pixel size and the overall detector size are independent of the X-ray wavelength in far-field imaging. They are proportional to the sample size to a certain power. In addition, the overall detector size is related to the pixel size for a perfectly coherent source as

$$L_D = \frac{Oa}{\delta} l_p \quad . \tag{7}$$

In other words, the number of pixels ($P^{\#}$) for each dimension is given by

$$P^{\#} = \frac{L_D}{l_p} = \frac{Oa}{\delta} \quad , \tag{8}$$

which is trivial. No source is perfectly coherent in time and space. In order to achieve the desired resolution δ, the temporal and spatial coherence requirements on the X-ray source are,

$$\frac{\lambda}{\Delta\lambda} \geq \frac{Oa}{\delta} = P^{\#}, \ \Delta\theta \leq \frac{\lambda}{2Oa}. \tag{9}$$

The demand on dynamic range for coherent imaging is very stringent. The amount of X-ray photon (dose) required to achieve certain spatial resolution δ is

---

[13] J. Miao, D. Sayre and H. N. Chapman, *Phase retrieval from the magnitude of the Fourier transforms of nonperiodic objects,* JOSA **15**, (1998) 1662.

found to be inversely proportional to the third [27] or fourth power of resolution.[14] In particular, the diffracted data has a dynamic range extending to about six orders of magnitude[12] and so the dynamic range of the detection system should also be correspondingly large. In other words, it would require at least 20 bit of resolution. Currently, most CCD or CMOS systems do not offer this, the required dynamic range is typically achieved by summing a large number of frames of data using cooled CCD or CMOS camera systems. The number of the frames required is given by the ratio of the desired dynamic range to the actual dynamic range of the detector. That is, for an imaging camera of 12 bit, corresponding to a dynamic range of 4096, more than 200 frames would be needed. Multiple frame imaging may not be an option for some of the MPDH experiments.

Functional requirement	Detector requirement	Notes
X-ray photons 10 keV	Si-based X-ray converter, Resolution limited to $\lambda/2$ = 62 pm	Si-based detector will not have sub-ns time response needed. InAs, GaInSb, InSb detectors at room temperature can deliver the fast time response needed. 1 pm = 10^{-12} m
Field of View 20 um x 20 um	Pixel size 57 um	
Resolution 10 nm	Pixel array 2000 x 2000 Detector size 113 mm x 113 mm	
Fraunhofer imaging	Detector-to-sample distance 12.9 m	Fresnel number 0.5 Oversampling ratio $0 = \sqrt{2}$

---

[14] M.R. Howells, T. Beetz, H.N. Chapman, et al., *An assessment of the resolution limitation due to radiation-damage in X-ray diffraction microscopy, J. Electron Spectroscopy and Related Phenomena* **170** *(2009) 4–12;*

Functional requirement	Detector requirement	Notes
Dynamic range $\sim 10^6$	20 bit data mode	

Functional requirement	Detector requirement	Notes
X-ray photons 50 keV	High-Z X-ray converter, Resolution limited to $\lambda/2$ = 12 pm	Such as InSb. Lowering the detector temperature at as high bias voltage as possible.
Field of View 100 um x 100 um	Pixel size 283 um	
Resolution 100 nm	Pixel array 1000 x 1000 Detector size 283 mm x 283 mm	
Fraunhofer imaging	Detector-to-sample distance 1610 m	Fresnel number 0.5 Oversampling ratio $O = \sqrt{2}$ (focusing lens may be required to reduce the distance or use near-field imaging)
Dynamic range $\sim 10^6$	20 bit data	

Functional requirement	Detector requirement	Notes
X-ray photons 50 keV	High-Z X-ray converter Resolution $\leq$ 12 pm	Such as GaAs or InSb

Field of View 1 mm x 1 mm	Pixel size 2830 um	Low-Z (such as Al or organic materials) samples only
Resolution 100 nm	Pixel array 1000 x 1000 Detector size 2830 mm x 2830 mm	
Fraunhofer imaging (*impractical*)	Detector distance 1.61×10^5 m	Fresnel number 0.5 Oversampling ratio $O = \sqrt{2}$ (alternative near-field imaging methods needed)
Dynamics range $\sim 10^6$	20 bit data	

2. X-ray interactions with matter

X-rays interact primarily with electrons. Interactions with nucleus that can lead to electron-position pair production, photo-fission, nuclear absorption such as (γ,γ), (γ,n), or (γ,p) processes, and others are conventionally classified as the γ-ray regime of photons,[15] and therefore negligible for X-rays at low intensities. Pair production and other nuclear interactions may become significant at high X-ray intensities when multi-photon effects arise. The threshold intensity for such effects may be estimated as follows, similar to multi-photon processes in longer wavelength regimes.[16] In an intense field, an electron may be accelerated to an energy comparable to the ponderomotive energy (in eV) $U_p = e^2 E_0^2/4m_e\omega^2 = 9.32 \times 10^{-20}$ $I\lambda^2$, with I in W/cm^2 being the coherent photon intensity, and λ the wavelength in nm. For 10 keV photons, the threshold intensity is 7×10^{26} W/cm^2 for $U_p \sim 1$ MeV, much higher than the anticipated MPDH X-ray intensities.

The three primary interaction mechanisms that are important for X-rays are photoelectric absorption, coherent scattering, and incoherent scattering. Even for absorption, an additional cascade of events are possible due to the fact that photoelectron can only take away a part of the photon energy, leaving the host

---

[15] G. F. Knoll, *Radiation detection and measurement, 3rd ed.,* (Wiley & Sons, 2000).
[16] P.B. Corkum, Phys. Rev. Lett. **71** (1993) 1994;

atom in an excited state. Such a cascade of events includes Auger electron emission, X-ray fluorescence, ionization and optical fluorescence.

Coherent scattering are also known as Thomson scattering (with free electrons), Rayleigh scattering (with bound electrons), classical scattering, or elastic scattering. In coherent scattering, X-ray photons do not lose their energies, but are only deflected due to electron oscillations. Incoherent scattering is also known as Compton scattering (with a free electron), in which photons lose a small fraction of energy and red-shifted from the incidental X-ray wavelength. X-ray interactions with matter are energy (wavelength) dependent. The range of interaction with an X-ray photon is measured by its wavelength, which is $\lambda = hc/E$. The uncertainly principle gives the same estimate of interaction range. For a 10 keV X-ray photon, the wavelength is 0.124 nm. A 50 keV X-ray photon has a wavelength of 2.48×10^{-2} nm. These wavelengths are comparable to the Bohr radius, 5.29×10^{-2} nm. Therefore, the particle-nature (or the 'point' nature) of photons or incoherent scattering is evident. In comparison, for photon wavelengths much greater than the Bohr radius, the wave-nature and therefore coherent scattering is more apparent. The wave-particle duality of X-ray scattering is described by quantum mechanics or quantum electrodynamics.[17] For scatterings off single free electrons, the Klein–Nishina formula gives the differential cross section of photons in the lowest order of quantum electrodynamics. For scatterings off multi-electron systems (Z>1), the frame-work of Dirac-Hartree-Fock (DHF) is frequently used.[18]

X-ray absorption and scattering increase with the atomic number to the zeroth order, Figure 6. To the first order, shell structures of electrons modify the cross sections periodically, in particular for low energy X-rays.[19] For most practical purposes, the details of X-ray scattering are captured in the differential and total cross sections for each individual processes, coherent scattering, incoherent scattering, or absorption.[20] The cross section data has been maintained by NIST and constantly updated based on latest measurements or calculations.[21] Absorption cross section dominates the total cross section, Figure 4 for carbon and Figure 5 for copper are shown as examples. When a sufficiently energetic X-ray photon is absorbed, photoelectrons may be ejected from any of the K-, L-, M-, … shells of an atom.[22] A third body, the nucleus, is needed for photoelectric absorption to conserve energy and momentum simultaneously; therefore, a free electron can not absorb a photon. It is found that absorption increases rapidly

[17]

[18] J. H. Scofield, *Theoretical photoionization cross sections from 1 to 1500 keV,* LLNL report UCRL-51326 (1973).

[19] E. Fermi and L. Marshall, *Interference Phenomena of slow neutrons,* Phys. Rev. **71** (1947) 666.

[20] J. H. Hubbell, *Review and history of photon cross section calculations,* Phys. Med. Biol. *51* (2006) R245-R262.

[21] "NIST X-Ray and Gamma-Ray Data," http://www.nist.gov/pml/data/xray_gammaray.cfm

[22] C. M.Davisson, *Interactions of γ-radiation with matter,* in K. Siegbahn (ed.) *Alpha-, Beta-, and Gamma-Ray Spectroscopy Vol. I* (North-Holland, Amsterdam, 1965) 37.

with the tightness of the electron binding and at energies above the K-shell binding energy, the K shell absorption contributes most.
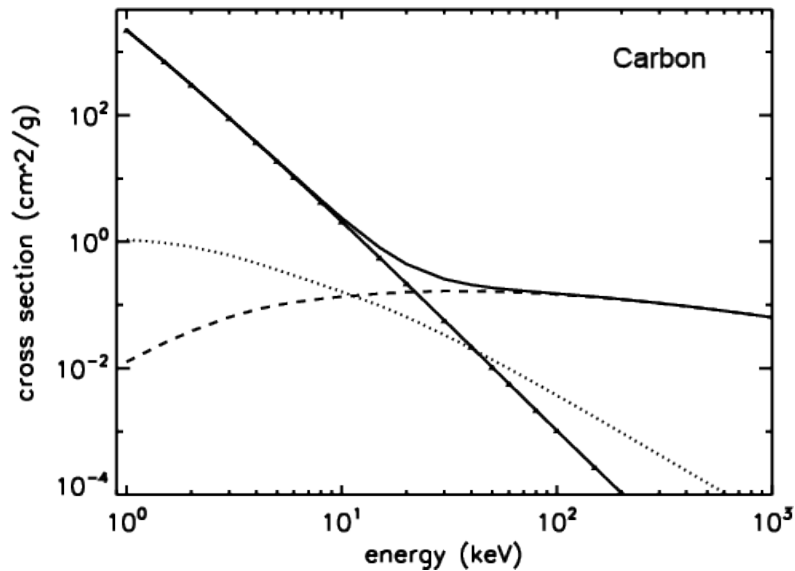
Figure 4. Total photon cross section σ_{tot} in carbon, as a function of energy, showing the contributions of different processes: τ, atomic photo-effect (electron ejection, photon absorption); σ_{coh}, coherent scattering (Rayleigh scattering—atom neither ionized nor excited); σ_{inch}, incoherent scattering (Compton scattering off an electron); [23]

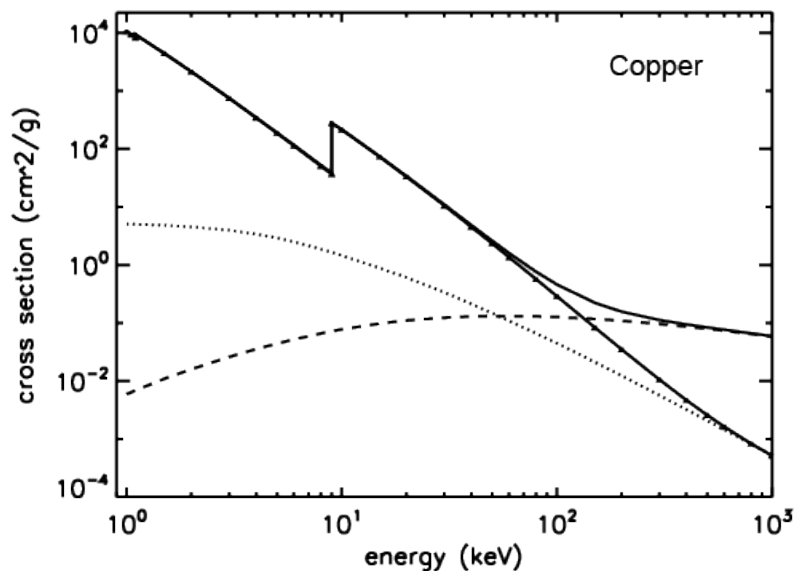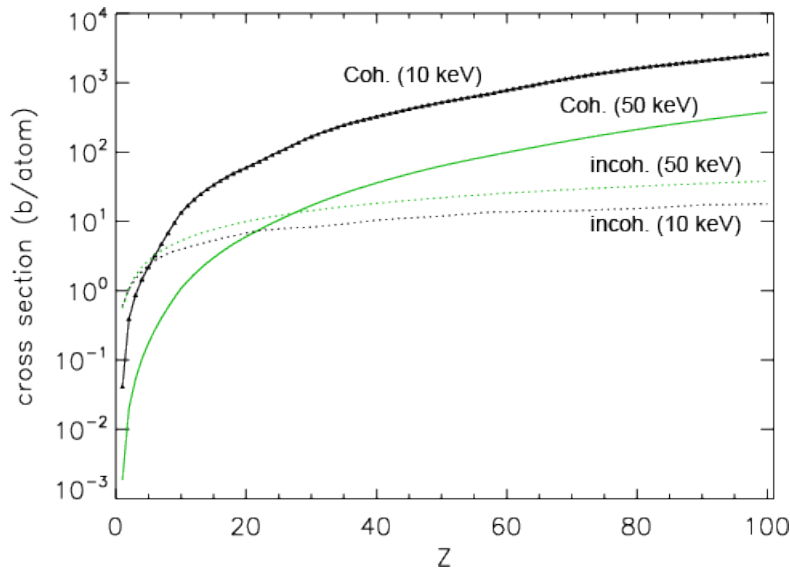**Figure 5. Total photon cross section σ_{tot} in copper, as a function of energy, showing the contributions of different processes as in Figure 5.** [23]

---

[23] http://www.nist.gov/pml/data/xcom/index.cfm ; J. H. Hubbell, et al., "Pair, Triplet, and Total Atomic Cross Sections (and Mass Attenuation Coefficients) for 1 MeV–100 GeV Photons in Elements Z = 1 to 100," *J. Phys. Chem. Ref. Data* **9**, 1023 (1980).

Figure 6. Coherent and incoherent cross sections as a function of atomic number for 10 keV and 50 keV hard X-rays.

Through interactions with its external (orbital) and intrinsic (spin) magnetic moments, an X-ray photon can also scattered off an electron magnetically.[24] The characteristic energy of such interactions is $\mu B \sim \mu_B B = eB\hbar/2m_e$, with B being the magnetic field of the photon. The magnetic scattering cross section is reduced from the coherent scattering cross section by a factor of $(\hbar\omega/m_e c^2)^2$, which corresponds to a factor of 3.83 x 10^{-4} for 10 keV X-rays, and 1.91 x 10^{-2} for 50 keV X-rays. Therefore, magnetic scatterings are not isolated from scattering due to electric interaction, will modulate electric interactions up to a few percent.

Collective scattering of X-ray photons, that is, scattering of a single X-ray photon by several electrons simultaneously, can only happen for electrons within an atom for hard X-rays. For soft X-rays, when the wavelengths can extend over multiple atomic spacing, Bragg scattering and Laue scattering are well known.

3. X-ray source and imaging

3.1 An ideal X-ray source for imaging of transients

An ideal X-ray source for imaging is a diffraction-limited coherent photon source, or a source with the smallest emittance possible. Such a source has the smallest volume in phase space, bounded by the uncertainty principle. A diffraction-limited source is spatially coherent with the lowest eigenmode number and is circular in both the real space and momentum space. The source coherence means that

[24] M. Blume, *Magnetic scattering of X rays,* J. Appl. Phys. **57** (1985) 3615.

both the intensity and phase information are available for imaging purposes.[25]

The complementary feature to spatial coherence is the bandwidth ($\Delta E/E$), which is a measure of spread in the momentum space and pulse length ($\Delta\tau$). The short pulse mode of operation of a light source for imaging is dictated by minimizing perturbations to atomic structure and motion of the sample (< 20 fs, atoms move on the order of hundreds of fs at room temperature), the time resolution needed and detector recovery time.

The maximum photon flux per pulse and therefore the peak power is limited by, for example, temperature rise in the sample,[26]

$$N_{max} = \frac{3k_B L^2}{E\sigma_{abs}}\Delta T_{max},\qquad(10)$$

where k_B is the Boltzmann constant, L^2 is the beam area, E is the photon energy, σ_{abs} is the absorption cross section per atom, and ΔT_{max} is the maximum allowable temperature rise. The density of material does not appear explicitly in Eq. (1) because its contribution to photon absorption cancels its effect on temperature rise.

The quality of an image is determined by the minimum number of photons needed per pixel over the readout noise. Since readout noise can be reduced to a few electrons these days, a few photons per pixel is normally sufficient for a good image. Five photons per pixel is proposed by Shen *et al.*[27] Howells et al.[14] proposed 25 photons per pixel to achieve a S/N of 5.

The proposed coherent linearly-polarized X-Ray source (XFEL) beam in MPDH has an energy bandwidth ($\Delta E/E$) 10^{-4} to 10^{-5}. The maximum beam divergence is 1 μrad. Diffracted image quality will also be determined by X-Ray detectors for both response rate as well as resolution. The goal of spatial resolution of three-dimensional measurements is at 1.0 micron, with a beam spot size up to 100 micron in diameter. The duration for a single image is less than 1 ps, the number of photons available per pulse is 10^{11}, assuming a coherent elastic scattering percentage of 1%, 10^9 photons will be available for imaging. The minimum pulse separation is 350 ps. About 30 images for a time window of 1.5 microsec would be generated.

In contrast to infrared, visible and UV light, which probe electronic or phonon states of a sample, X-rays map electron density distribution of a sample. The positions of the atoms, and therefore structures, are inferred from the electron distribution. Historically, X-rays were used first for radiography, and later in phase

[25] Polarized source provides additional information that may be useful for imaging.

[26] D. H. Bilderback, J. D. Brock, D. S. Dale et al., *Energy recovery linac (ERL) coherent hard X-ray source,* New. J. Phys. **12** (2010) 035011.

[27] Q. Shen, I Bazarov and P. Thibault, *Diffractive imaging of nonperiodic materials with future coherent X-ray sources,* J. Synchrotron Radiat. **11** (2004) 432.

contrast imaging[28] and holography. X-ray radiograph methods are based on differential absorption of a sample. X-ray attenuation depends on the material composition along the path as well as the total length of the path. The intensity pattern of the transmitted photons records the absorbing materials distribution (line-integrated density weighted by the absorption cross section, $\int \rho \sigma dx$) within the sample. Absorption is also wavelength dependent. In visible light, differential absorption of different wavelengths gives rise to colors. Except for X-ray radiography, all other methods utilize both the intensity and phase information of scattered X-rays. Nano-second resolution X-ray diffraction experiments have been used since the 1980's.[29] High resolution X-Ray diffraction techniques and computed micro-tomography is a mature experimental tool which has been performed on metallic materials at the Advance Photon Source (APS).[30] Computed micro-tomography is also now readily available for use in the materials science laboratory. Recently a program has been initiated to integrate High Energy X-Ray Diffraction Microscopy with computed micro-tomography to post analyze damaged plate impact samples. They will also be examining damage evolution in-situ during quasi-static tension.

3.2 Phase contrast imaging

Radiography methods are most effective when there is a large gradient in absorption along different paths of the illumination. In other words, the imaginary part of the refractive index is a sensitive function across the sample. When the absorption gradient is not so large or even negligible, for example, in a transparent specimen or a sample with a relatively flat absorption profile, phase contrast methods can be used. As the energy of the radiation increases, the image contrast due to absorption diminishes. By comparison, the phase shift, if it can be rendered visible, remains relatively high. For example, for 1 nm radiation, approximately 3 μm of carbon produces a 2π phase shift and 50% absorption. If the wavelength is decreased to 0.1 nm, 3 mm of carbon is required to produce 50% absorption while only 30 μm is required to produce a 2π phase shift. Thus, for imaging with hard x rays there is a considerable premium on being able to use phase as the contrast mechanism.[31]

Ideally, phase contrast imaging needs a coherent source, which supplies a *uniform*[32] phase field spatially and temporarily. The relative phase along different path can be combined and compared at the detector afterwards. Basically small

---

[28] S.W. Wilkins, Australian Patent No. PM0583/93 (1993); T. J. Davis, D. Gao, T. Gureyev, A. W. Stevenson, and S.W. Wilkins, Nature (London) **373**, (1995) 595; S. W. Wilkins, T. E. Gureyev, D. Gao, A. Pogany, and A. W. Stevenson, *Phase-contrast imaging using polychromatic hard X-rays,* Nature **384** (1996) 335.

[29] A. Rousse, C. Rischel, and J.-C. Gauthier, *Femtosecond X-ray crystallography,* Rev. Mod. Phys. **73** (2001) 17; Larson, B. C., C. W. White, T. S. Noggle, et al., Phys. Rev. Lett. **48** (1982) 337.

[30] Mat. Sci. Eng. A-Struct. 641, 483 (2008); Appl. Phys. Let. 96, 043122 (2010); Corrosion Sci. 50, 3455 (2008).

[31] K. A. Nugent, T. E. Gureyev, D. F. Cookson, D. Paganin and Z. Barnea, *Quantitative Phase Imaging using Hard X-rays,* PRL **77**, (1996) 2961.

[32] The relative phase from one point in the 4-dimensional space (**r**, t) to another (**r'**,t') is known.

phase shifts are converted into amplitude change in detection and improve image contrast. Similarly, other mechanisms of X-ray interaction with matter, reflection, scattering, diffraction can result in contrast due to the differences in interaction details. Phase contrast illumination was invented by F. Zernike in the 1930s, for which he received the Nobel prize in physics in 1953.

Using an incoherent source, such as X-rays from a plasma or a e-beam interaction with a target, the source size (D), the object size being illuminated (a), the distance of the object from the object (Z_s), and the wavelength must satisfy[33]

$$\frac{Da}{z_s} \leq \frac{\lambda}{4},$$ (11)

The optical properties of materials, in particular, the index of refraction for X-rays, are related to the scattering of the individual atoms by[34]

$$n = 1 - \frac{r_e \lambda^2}{2\pi} \sum_i n_i f_i,$$ (12)

where r_e is the classical electron radius, λ the X-ray wavelength, and n_i the number of atoms of type i per unit volume. The atomic scattering factor f normally has both a real and an imaginary component, $f = f_1 + if_2$. The imaginary part is derived from the photo-absorption cross section

$$f_2 = \frac{\sigma}{2r_e \lambda},$$ (13)

The real part of the atomic scattering factor is related to the imaginary part by the Kramers-Kronig dispersion relation. For X-ray and higher energy photons, f_1 approaches a limit given by $f_1 \sim Z^* \sim Z - (Z/82.5)^{2.37}$.

3.3 Coherent diffractive imaging

In the early 1980's, D. Sayre recognized the benefits of using coherent X-ray diffraction imaging (CDI) for noncrystalline specimens.[35] Periodic arrangement of atoms in crystals amplifies the signal diffracted from the unit cell, resulting in discrete Bragg peaks with high intensity. For nonperiodic or noncrystalline samples, diffracted light smears out and produces a seemingly continuous diffraction light pattern. For an object of finite size, it can be proven theoretically that the diffracted light has a finite bandwidth,[36] or the diffracted light patterns are

[33] A. Lipson, S. G. Lipson, and H. Lipson, *Optical Physics (4th Ed.)* (Cambridge University Press, 2011) p. 204.

[34] E. M. Gullikson, *Atomic Scattering Factors,* in X-ray Data Booklet; http://xdb.lbl.gov/.

[35] D. Sayre, in *Imaging processes and Coherence in Physics,* M. Schlenker et al. (eds.) Springer-Verlag, New York (1980); Q. Shen, Q. Hao and S. M. Gruner, *Macromolecular phasing,* Phys. Today (Mar. 2006) 46.

[36] C. E. Shannon, "Communication in the presence of noise", Reprint as classic paper in: *Proc. IEEE, vol. 86, no. 2, (Feb. 1998)*

peudo-continuous. Oversampling of the diffracted light pattern, with spatial frequencies higher than the largest frequency in the pattern (the Nyquist frequency), allows one to recover all the spatial frequencies, which can then be used to reconstruct the structure of the object with an inverse Fourier transform. From the classical physics point of view, a structure measurement at a certain time corresponds to solve for the 3N coordinates of the atomic constituents, where N is the number of atoms in the object. In other words, whether the 3N positions are periodic or not, the information content of the finite object is only finite. Because of the over-sampling requirement over a large area, a large number of photons would be needed for CDI. A noisy background will require even more illumination. In CDI of static and in particular dynamic objects, the limited coherent light output is a significant barrier to obtaining shorter exposure times.[37]

Coherent X-rays diffraction imaging was demonstrated in the late 90's and is now in common use in synchrotron sources.[38] Recently, a new method called ankylography, in which a single X-ray beam passed through the sample and the diffracted image was captured on an Ewald sphere.[39]

4. X-ray detectors, then and now

An X-ray detector is a material structure or an arrangement of atoms that measures X-ray flux or power. Either way, the energy of an X-ray photon or a sum of energies is converted into an electric (charge, voltage or current) signal and recorded. Other properties of the photon, such as its polarization and its phase, are normally not harvested directly for detection. It is known, however, that a photoelectron is injected preferentially along the electric vector of the incident X-ray photon.[40] At X-ray energies up to 50 keV, the predominant X-ray interaction process is photoelectric absorption by electrons, when full or partial energy deposition in the detector from the X-ray photon is possible. The photoelectron only carries away a part of the X-ray photon energy, $E_{ph} = h\nu - W$. The work function W has two contributions, $W = B + W_0$, W_0 is due to inter-atomic potential, while B is from the atomic Coulomb potential where the photoelectron originally resides.[41] $W_0 << B$ since the inter-atomic potential is much weaker than the Coulomb potential near the nucleus. B corresponds to the inner-shell ionization potential of an atom, K-, L-, M-, … with decreasing probability as the shell number increases. B can be a significant fraction of the incidental X-ray energy and induce additional secondary effects, including additional emissions of longer wavelength X-rays (Fluorescent X-rays), UV and visible photons or Auger

[37] B. Abbey, L. W. Whitehead, H. M. Quiney et al., *Lenseless imaging using broadband X-ray sources,* Nat. Photonics **5**, (2011) 420.
[38] Miao et al, Nature (1999).
[39] Nature **463**, 214 (2010)
[40] H. Tsunemi, *Development of the X-ray CCD in Japan,* NIMA **541** (2005) 295.
[41] C. Grupen and B. Shwartz, *Particle detectors,* 2nd ed. (Cambridge University Press, 2008) p. 33.

electrons. Fluorescence yield is used to measure the fraction of fluorescence X-ray emitted for each photoelectric vacancy.[42] The fluorescence yield depends on the atomic number (Z) and the shell number. An empirical law of the form[43]

$$y_x = \frac{Z^4}{A_x + Z^4}$$

(14)

has been found. For the K shell X-rays, $A_i = 10^6$, and 10^8 for the L shell. It can be seen that up to potassium (Z=19) more than 90% of the K-emission takes place via Auger emission.[44] The probabilities for X-ray fluorescence and Auger emission are equal for Germanium (Z=32).

If the fluorescent X-ray is photo-electrically re-absorbed by the detector, then the fully energy absorption is achievable, otherwise only partially energy absorption is obtained. Compton scattering can only transfer a fraction of the photon energy to an electron up to the Compton edge, $2 (h\nu)^2 / (m_e c^2 + 2 h\nu)$ and therefore can also be useful for detection. For 10 keV photons, the Compton edge is 0.377 keV. For 50 keV, the Compton edge is 8.2 keV. Coherent scattering of X-rays does not deposit any energy in the detector, but momentum conservation requires some re-arrangement in the scattering host and therefore, some potential detection mechanism may be arise. So far, such mechanism has not been explored for detection.

A highly efficient X-ray detector does not require full absorption of the incoming X-ray photon energy. However, it is necessary that each absorption must turn into a recordable signal. Therefore, an efficient detector absorbs most of the incoming X-ray photons, which is important to MPDH. The differential absorption process in a compound is described by

$$dI(\omega) = I(\omega) \sum_i w_i \mu_i \rho dx ,$$

(15)

where $I(\omega)$ stands for the X-ray intensity for certain frequency on the detector and dI for the change of intensity going through an areal density ρdx of the compound. ρ is the compound mass density. The index i stands for the i-th atomic species of the compound, w_i being the corresponding atomic weight fraction in the compound molecule,

[42] J. H. Hubbell et al, *A Review, Bibliography, and tabulation of K, L, and Higher atomic shell X-ray fluorescence yield*, J. Phys. Chem Ref. Data **23** (1994) 339; X-Ray Data Booklet Sec. 1.3;

[43] E. P. Bertin, *Principles and Practice of X-Ray Spectrometric Analysis,* (Plenum Press, New York, 1975).

[44] G. Ertl and J. Kuppers, *Low Energy Electrons and Surface Chemistry,* (VCH, Weinheim, 1985).

$$w_i = \frac{m_i A_i}{\sum_k m_k A_k} \,, \tag{16}$$

therefore satisfying $\sum_i w_i = 1$. m_i's are the number of atoms in the compound molecule for the ith species. For example, in uranium oxide (UO_2), $m_1=1$ for uranium and $m_2=2$ for oxygen. μ_i is the mass attenuation coefficient, which is determined by the total cross section of X-ray interaction and the density,

$$\mu_i = \frac{N_0}{A_i} \sum_k \sigma_k \,, \tag{17}$$

where the sum is over various absorption and scattering cross sections, N_0 is the Avogadro number and A_i the molar weight. Since none of the material properties is X-ray intensity dependent, the Eq. (2) can be integrated, resulting in an exponential decay of the X-ray intensity as detector size increases.

Below, we show the attenuation of X-ray photons with energies of 10 keV and 50 keV as a function of the atomic number Z. The photoelectric absorption cross section scales as $Z^n \lambda^3$, where λ is the X-ray wavelength and Z is the atomic number of the detector gas and n ~ 4–5. The corresponding coherent scattering cross sections (dotted lines) and the total cross section excluding coherent scattering (dashed lines) are shown alongside.

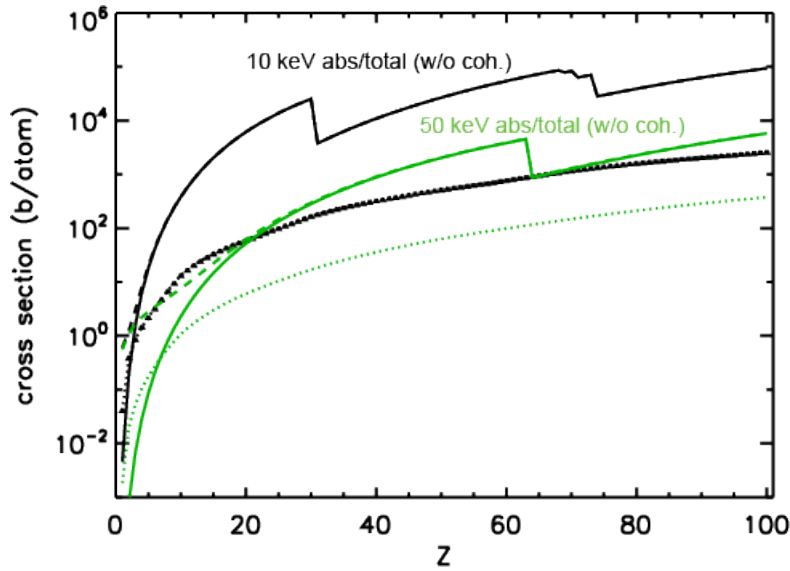**Figure 7. Photoelectric absorption cross section as a function of atomic number for 10 keV and 50 keV X-rays (solid lines).**

For 10 keV X-ray absorption, the first edge happen from Zn (Z=30) transition to Ga (Z=31), which can be derived from the relation $(Z-s)^2 E_{b0} = E_x$, with E_{b0} =13.6 eV, E_x=10 keV and s~3. For 50 keV, the same relation gives Z=63 (Eu), with a drop in cross section to Z=64 (Gd).

Half-absorption thicknesses of a few typical elements used in X-ray detectors, defined as T = ln2/$\mu\rho$, are tabulated here for 10 keV and 50 keV X-rays.

	Z	ρ (g/cc)	μ @ 10 keV (cm^2/g)	T @ 10 keV Thickness (μm)	μ @ 50 keV (cm^2/g)	T @ 50 keV Thickness (μm)
Be	4	1.85	0.4229	8.9e+3	1.919e-3	1.95e+6
C (graphite)	6	2.1	2.076	1.6e+3	1.042e-2	3.2e+5
C (diamond)	6	3.5	2.076	954	1.042e-2	1.9e+5
Si	14	2.33	33.15	90	0.2307	1.3e+4
Ge	32	5.32	35.71	36	3.044	428
Cd	48	8.65	121.8	6.58	9.359	85.6
Te	52	6.24	147.4	7.5	11.02	101
I	53	4.93	159.7	8.8	11.87	118
Bi	83	9.78	130.9	5.4	7.613	93

Detection of 50 keV photons requires at least ten times thicker detectors for similar efficiencies to 10 keV detectors. Therefore, 50 keV X-ray can require larger detector volumes,[45] resulting in correspondingly higher background. In this energy range, most detectors in space applications are either scintillators or solid-state detectors to take advantage of their large mass densities.[46]

The size of the detector is also affected by the photoelectron range, to a less extent, for electron energies up to tens of keV. In this energy range, which is much less than the critical energy for the stopping material, E_c ~ 800MeV/(Z+1.2),[47] the slowing-down of an electron is due to excitation and ionization of bound electrons, just as for the heavy particles. The energy loss per unit distance [in the unit of MeV/(g cm^{-2})] is described by the Bethe-Bloch formula[48] and its corrections (Koch-Motz formula) for low energy (10 keV to 2

---

[45] This is not strictly true. One can use the time-of-flight setup (two detector/scintialltors in series) to take advantage of the high penetrating power of the hard X-rays.
[46] D. M. Smith, *Hard X-ray and γ-ray detectors,* arXiv:1010.4069v1 (2010).
[47] http://pdg.lbl.gove/2010/reviews/.
[48] Particle Data Group, http://pdg.lbl.gov; W. Blum, W. Riegler, and L. Rolandi, *Particle detection with drift chambers,* (Springer, 2008).

MeV) electrons.[49] The electron range can be estimated as R = ∫dE / dE/dx. Since the electron trajectory is a not a straight line, this estimate of electron range is an upper limit. For electron energies below ~ 5 keV, the Bethe-Bloch formula is inadequate for calculating the electron energy loss in a solid.[50] But from detection perspective, the ranges of electrons are on the order of 1 micron or less, which are small compared with the X-ray absorption length, and do not change detector size significantly. Although photoelectron range does not affect the detector sizes dramatically, it limits the size of detectors when they are used directly to generate detector signals. The following table is based on Ref. 49. dE/dx shown is the sum of the ionization loss and bremsstraghlung loss, in which ionization loss dominates the slowing-down of the electrons.

	Z	ρ (g/cc)	dE/dx @ 10 keV (MeV cm^2/g)	R @ 10 keV (g/cm^2)	R @ 10 keV (μm)	dE/dx @ 50 keV (MeV cm^2/g)	R@ 50 keV (g/cm^2)	R @ 50 keV (μm)
Be	4	1.85	18.8	2.65e-4	1.43	5.46	5.17e-3	27.9
C (gra.)	6	2.1	20.1	2.48e-4	1.18	5.91	4.80e-3	22.9
C (dia.)	6	3.5	20.1	2.48e-4	0.71	5.91	4.80e-3	13.7
Si	14	2.33	16.9	2.95e-4	1.27	5.19	5.53e-3	23.7
Ge	32	5.32	12.5	3.99e-4	0.75	4.05	7.19e-3	13.5
Cd	48	8.65	10.9	4.60e-4	0.53	3.65	8.07e-3	9.3
Te	52	6.24	10.1	4.94e-4	0.79	3.44	8.61e-3	13.8
I	53	4.93	10.3	4.85e-4	0.98	3.51	8.44e-3	17.1
Bi	83	9.78	8.45	5.92e-4	0.60	3.05	9.87e-3	10.1

4.1. X-ray detection methods

All X-ray detectors have a few common building blocks, independent of their construction details, as illustrated in Figure 8. They may include X-ray

---

[49] L. Pages, E. Bertel, H. Joffre and L. Sklavenitis, *Energy loss, range, and bremsstrahlung yield for 10 keV to 100 MeV electrons in various elements and chemical compounds*. Atomic Data **4** (1972) 1-127.
[50] X-ray Data Booklet, online, http://xdb.lbl.gov/;

capture/conversion, amplification, recording and readout. On the top of these, there are timing and gating units. Interfaces and interconnects are also important to integrate different blocks and data transmission. One can easily draw a parallel between X-ray detection with information or signal processing. From signal processing point of view, X-ray capture/conversion corresponds to the function of a transducer. The rest of the blocks and their functions are the same as other signal processing devices, such as a micro-processor in a computer.
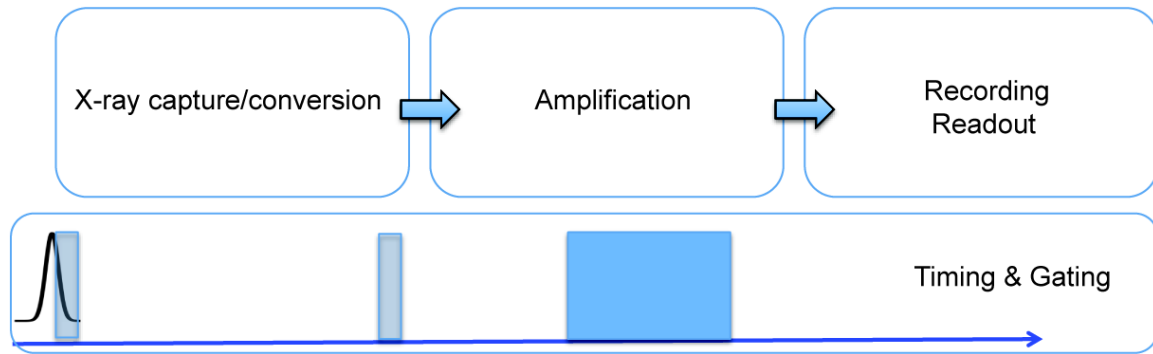
Figure 8. Building-blocks of X-ray detectors. Not explicitly shown are interfaces and inter-connects (such as tapered fibers) in-between the blocks. Detectors for charged particle radiography and imaging also have the same components with some minor modifications, mostly at the front end (the capture and signal conversion block).

Here we limit our discussions to methods that are either based on *direct photoelectron* conversion when the photoelectrons from the X-ray absorption are detected directly or *secondary photoelectron* conversion when X-ray photons produce a shower of longer wavelength photons in scintillating materials before the photoelectric conversion. Direct photoelectric conversion method based on primary electrons includes proportional counters,[51] silicon, germanium, and other semiconducting detectors, and streak cameras.[52]

Therefore, semiconductors and scintillators as the X-ray capture/conversion media are emphasized here. This approach leaves out traditional uses of silver-bromide-based X-ray films, novel uses of materials such as superconductors, superfluids, and novel uses of phase transitions, such as cloud chambers and bubble detectors.[53] The main reason for this exclusion is that the time responses of these detectors are too slow to be useful to MPDH. This, however, should not preclude the use of cryogenic technologies for MPDH. In particular, operations of semiconductor detectors at cryogenic temperatures can achieve faster time response due to drastic increase in electron mobility. For example, at room temperature, CdS has an electron mobility around 300 cm^2 V^{-1} s^{-1}. At 77K, the electron mobility in CdS increases to 1700 cm^2 V^{-1} s^{-1}.[54] At 4.2 K, the electron

[51] J. E. Trumper and G. Hasinger, (eds.) *The Universe in X-rays*, (Springer, 2008)*;* G. W. Fraser, *X-ray Detectors in Astronomy* (Cambridge University Press, 2009);

[52] J. Larsson, Z. Chang, E. Judd et al., *Ultrafast x-ray diffraction using a streak-camera detector in averaging mode.'* Opt. Lett. **22** (1997) 1012.

[53] G. F. Knoll, *Radiation detection and measurement* (3rd., John Wiley & Sons, Inc. 2000)*.* Chap. 19.

[54] Moore, A. R., Smith, R. W.: Proc. 7th Int. Conf. Physics Semicond., Paris, 1964, 575.

mobility increases further to 3.6 x 10^4 cm^2 V^{-1} s^{-1}.[55] Other semiconductors or compound semiconductors follows similar trend as will be discussed below.

The quantum efficiency decreases rapidly for the same type of photocathode as the wavelength of an X-ray decreases. While increasing the thickness of the photocathode is an obvious choice for better efficiency, the limited ranges of the photoelectrons within the photocathode become a conflicting issue. Compared with detectors in medical applications of X-rays and studies of materials or biological samples through high-repetition rate coherent photons in synchrotron or FEL facilities, MPDH is far more challenging because of shorter X-ray wavelength, faster time response combined with very fine spatial resolution needed in a single-shot.

Charge or current amplification (multiplication) is normally implemented in the detection chain for better detection sensitivity, energy resolution and S/N. Light amplification is much harder than electron multiplication and is yet to be seen for X-ray detection. Besides electrical amplification, photomultipliers, avalanche photodiodes, and Micro-Channel-Plates (MCPs) are examples of electron signal amplification devices.

Pixilated digital recording devices, in particular CCD cameras,[56] and lately CMOS cameras are the mainstream of recording and readout. Pixel array detectors (PADs)[57] and pnCCDs[58] have been developed to deal with both the detection efficiency and charge collection over a length much greater than the stopping ranges of photoelectrons. Compared with conventional CCDs, which normally needs only a few micrometer of surface depletion to visible light, tens to hundreds micrometers of depletion region is created for improved X-ray capture efficiency in PADs and pnCCDs. The depletion layer also serves as the charge pair separation and transfer region.

Phosphors and scintillators

A phosphor is a material that exhibits luminescence,[59] a phenomenon when a small fraction of the atoms of a bulk, called luminescent centers, emits light.**[60]** Fluorescent materials, where the emission decay takes place over nanoseconds (as opposed to longer times) and does not involve metastable states of electrons (allowed transitions, or $\Delta S=0$), is a part of the phosphor family. Most phosphors have a transparent microcrystalline matrix (a host) and an activator, as in a formula like Zn_2SiO_4:Mn(0.02), where the first part is the matrix (Zn_2SiO_4), and the second part the activator (Mn) with a molar quantity per mole of matrix in the

[55] Shimada, H., Masumi, T.: J. Phys. Soc. Jpn. **62** (1993) 3203.

[56] http://www.photometrics.com

[57] S. M. Grunner, M. W. Tate and E. Eikenberry, *Charge-coupled device area X-ray detectors,* Rev. Sci. Instrum. **73** (2002) 2815.

[58] J. E. Trumper and G. Hasinger (eds.) The Universe in X-Rays, (Springer-Verlag, Berlin, 2008) 51.

[59] D. Curie, Luminescence in Crystals. (Wiley, London, 1963); H. W. Leverenz, An Introduction to Luminescence of Solids. (Dover, New York, 1968)

[60] G. Blasse and B. C. Grabmaier, Luminescent Materials. (Springer, Berlin, 1994).

raw material mixture.[61] In additional to the properties in the table, other properties that are important to X-ray detection are short emission decay time, durability and dispersion. Short emission decay time allows a phosphor for repetitive uses without residue after-glow. Durability allows a phosphor to last in ambient without degradation due to, for example, moisture. To obtain a homogenous phosphor layer on a surface, the phosphor must disperse well in the coating slurry without forming coagulated particles.

phospher	Emission spectrum			X-ray absorption		Material structure	
	Emission color	Peak wavelength (nm)	Emission efficiency (%)	Effective atomic number	K-edge (keV)	Specific gravity	Crystal structure
$BaFCl:Eu^{2+}$	violet	380	13	49.3	37.38	4.7	Tetragonal
$BaSO_4:Eu^{2+}$	violet	390	6	45.5	37.38	4.5	Rhombic
$CaWO_4$	Blue	420	5	61.8	69.48	6.1	Tetragonal
$Gd_2O_2S:Tb^{3+}$	Green	545	13	59.5	50.22	7.3	Hexagonal
$LaOBr: Tb^{3+}$	Whitish-blue	420	20	49.3	38.92	6.3	Tetragonal
$LaOBr: Tm^{3+}$	Blue	360,460	14	49.3	38.92	6.3	Tetragonal
$La_2O_2S: Tb^{3+}$	Green	545	12.5	52.6	38.92	6.5	Hexagonal
$Y_2O_2S: Tb^{3+}$	Whitish-blue	420	18	34.9	17.04	4.9	Hexagonal
$YTaO_4$	UV	337		59.8	67.42	7.5	Monoclinic
$YTaO_4:Nb$	Blue	410	11	59.8	67.42	7.5	Monoclinic
$ZnS:Ag$	Blue	450	17	26.7	9.66	3.9	Hexagonal
$(Zn,Cd)S:Ag$	Green	530	19	38.4	9.66/26.7	4.8	Hexagonal

Table: A list of some X-ray phosphors and their properties.[62]

Scintillation is an example of radioluminescence, the phenomenon by which luminescence is produced in a material by the bombardment of ionizing radiation such as X-rays. Scintillators may be organic and inorganic solid, liquid, and gas. An "ultimate" scintillator is one that has high density and atomic number, high

---

[61] W. M. Yen, S. Shionoya and H. Yamamoto (eds.) *Fundamentals of Phosphors, (CRC Press, Boca Raton, 2007).*

[62] N. Miura, *Phosphors for X-ray and ionizing radiation,* in W. M. Yen, S. Shionoya and H. Yamamoto (eds.) *Practical applications of Phosphers (CRC Press, Boca Raton, 2007) p. 286.*

light output, short decay time without afterglow,[63] convenient emission wavelength, mechanical ruggedness, radiation hardness, and low cost.[64]
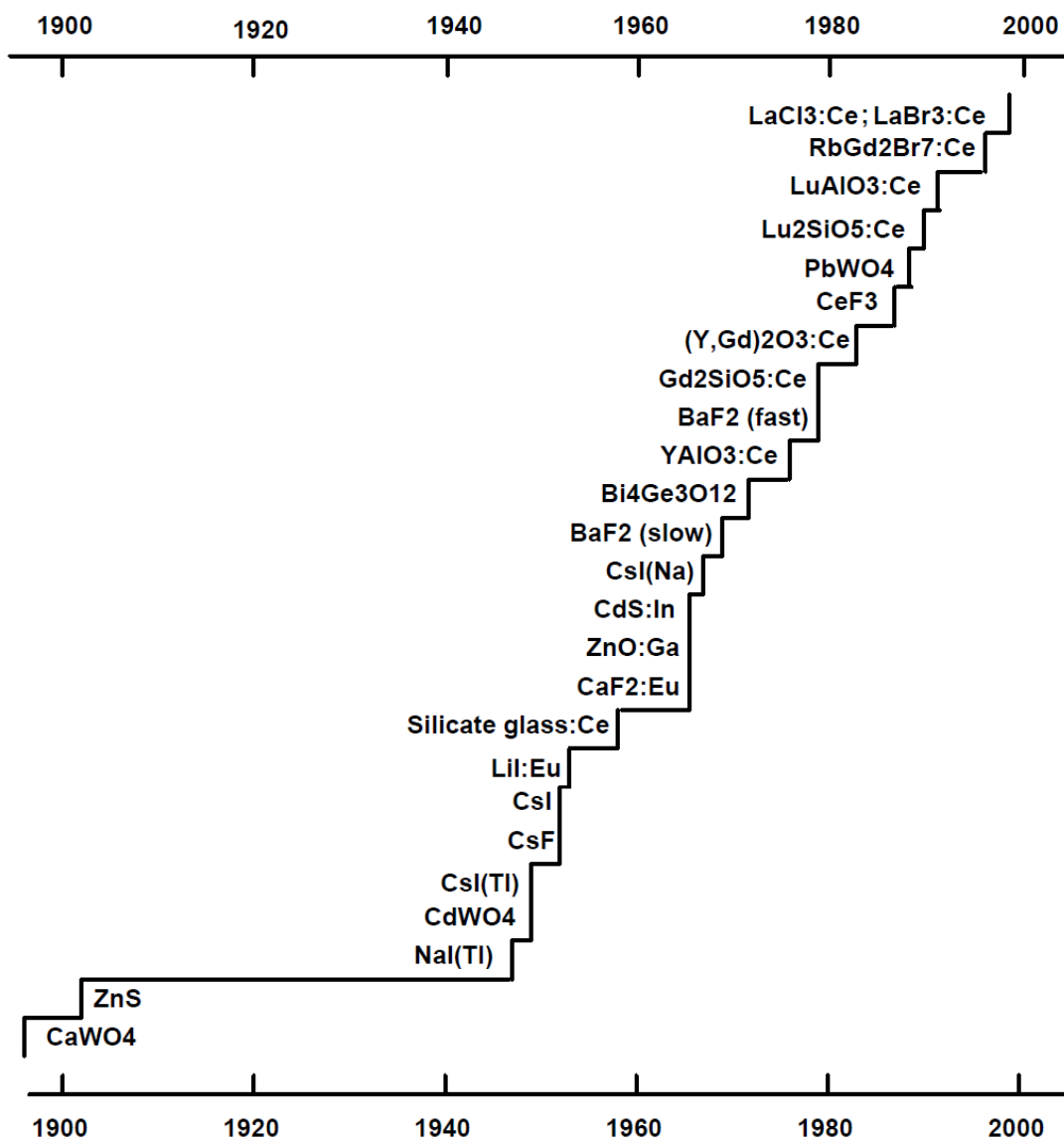
Figure 9. History of the discovery of major inorganic scintillator materials.[65]

Pure CsI scintillator (with decay time constant of 16 ns) is a typical photocathode in the X-ray range of wavelengths. The only other scintillators that have a faster decay constant are BaF_2 (fast component, 0.7 ns) and BC-408 plastic (2.1 ns). In summary, most fast crystals have a rising time at a level of 30 ps. Laboratory measurements of time response are often dominated by the response time of

---

[63] Afterglow is related to metastable excited electronic states.

[64] W. W. Moses, *Current trends in scintillator detectors and materials,* Nucl. Instrum. Meth. Phys. Res. A **487** (2002) 123.

[65] M. J. Weber, *Inorganic scintillators, today and tomorrow,* J. Lumin. **100** (2002) 35.

photo-detectors and readout electronics, and also affected by light propagation.[66] Time resolution of a scintillator based system can be optimized by choosing (1) bright and fast scintillators, (2) fast photo-detector with high gain and low jitter and (3) appropriate time pick off or trigger threshold. The achievable FWHM time resolution is 200 and 300 ps respectively for non-hygroscopic crystals BaF_2 and LSO/LYSO. In comparison, the state-of-the-art Time-of-Flight (TOF) positron emission tomography (PET) is about 100 ps by using $LaBr_3$.[66]
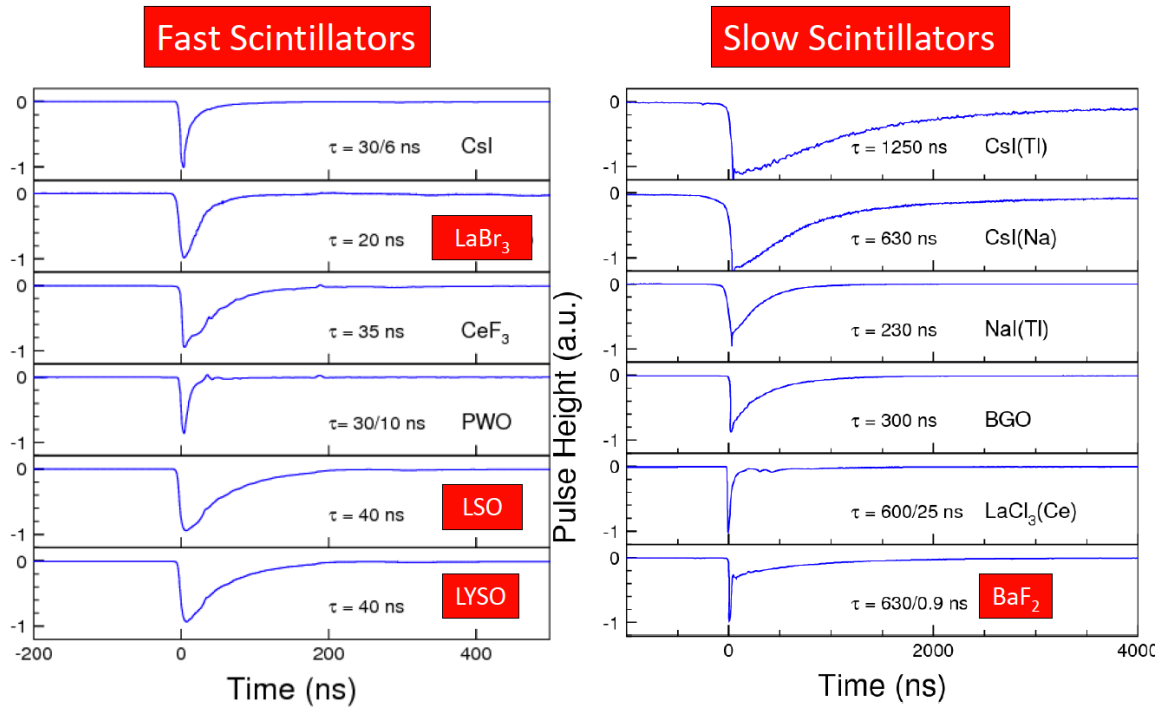

Figure 10. A comparison of scintillator decay time.[66]

[66] R.-Y., Zhu (Caltech), *Crystal Scintillators and Time resolution.* Presented in Conf. on Factors that Limit Time Resolution in Photodetectors, U. Chicago, April 28-29, (2011)

Crystal	NaI(Tl)	CsI(Tl)	CsI	BaF$_2$	CeF$_3$	BGO	PbWO$_4$	LSO(Ce)
Density (g/cm^3)	3.67	4.51	4.51	4.89	6.16	7.13	8.3	7.40
Melting Point (°C)	651	621	621	1280	1460	1050	1123	2050
Radiation Length (cm)	2.59	1.86	1.86	2.03	1.70	1.12	0.89	1.14
Molière Radius (cm)	4.13	3.57	3.57	3.10	2.41	2.23	2.00	2.07
Interaction Length (cm)	42.9	39.3	39.3	30.7	23.2	22.7	20.7	20.9
Refractive Index[a]	1.85	1.79	1.95	1.50	1.62	2.15	2.20	1.82
Hygroscopicity	Yes	Slight	Slight	No	No	No	No	No
Luminescence[b] (nm)	410	560	420	300	340	480	425	420
(at Peak)			310	220	300		420	
Decay Time[b] (ns)	245	1220	30	650	30	300	30	40
			6	0.9			10	
Light Yield[b,c]	100	165	3.6	36	7.3	21	0.30	85
			1.1	4.1			0.077	
d(LY)/dT[b,d] (%/°C)	-0.2	0.4	-1.4	-1.9	~0	-0.9	-2.5	-0.2
				0.1				
Experiment	Crystal Ball	CLEO BaBar BELLE BES III	KTeV	TAPS	-	L3 BELLE	CMS ALICE PrimEx Panda	SuperB

a At the wavelength of the emission maximum.
b Top line: slow component, bottom line: fast component.
c Relative light yield of samples of 1.5 X$_0$ and with the PMT quantum efficiency taken out.
d At room temperature.

Figure 11. Properties of some crystals that can be used in Hard X-ray detectors.[67]

Semiconductors

Silicon is a popular material to detect visible light and soft X-rays. Due to the low absorption coefficient of X-rays in silicon (Z=14), Si-based converter is, in practice, limited to energies below 60 keV. The achieved performance of these devices depends on the size of the detector. At room temperature, the best energy resolution achieved is around 1 keV (for 6 keV X-rays). For MPDH and other hard X-ray detection, high-Z semiconductors are desirable. There are a large number of choices from II-VI group of the periodical table. Besides Z, another important criterion is electron and hole mobility. Higher electron mobility corresponds to faster time response by the detector and higher frame rate.

In solid, thermal motions of electrons do not given rise to any current. In an external field, electron drift motion gives rise to a directed current. Electron mobility (μ_e) in semiconductor, and similarly hole mobility, is a measure of the electron drift motion in response to an external field,

$$V_d = \mu_e E. \tag{18}$$

Such a linear dependence on E is normally applicable to low field. The mobility also be expressed in terms of collision frequency (ν) as

[67] R.-Y. Zhu, *Precision Crystal Calorimeters in High Energy Physics: Past, Present and Future,* SPIE **7079** (2008)

$$\mu_e = \frac{e}{m^* v}.\qquad(19)$$

Electron mobility is also strongly dependent on doping. For a doped material,

$$\frac{1}{\mu_e} = \sum_k \frac{w_k}{\mu_{ek}},\qquad(20)$$

with w_k being the fraction of each component of the atomic composition. This is also known as Matthiesen's rule.
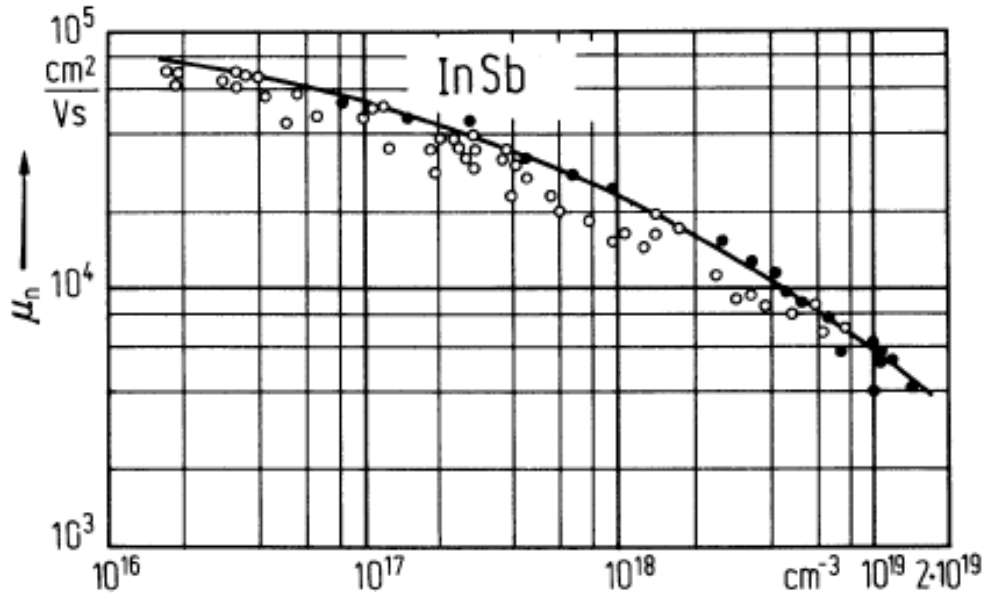
Figure 12. InSb. Electron mobility vs. electron concentration (a) at room temperature. Solid line, theoretical value from [68].

Hole mobility is always smaller than electron mobility for the same material because of the larger effective mass of a hole. Using silicon as an example,[69] The electron, as well as the hole, mobility can be expressed in the form

---

[68] Litwin-Staszewska, E., Szymanska, W., Piotrzkowski, R.: Phys. Status Solidi (b) 106 (1981) 551.
[69] D. M. Caughey and R. E. Thomas, *Carrier mobilities in silicon empirically related to doping and field,* Proc. IEEE **55** (1967) 2192.

$$\mu = \frac{\mu_{max} - \mu_{min}}{1 + (N/N_0)^\alpha} + \mu_{min} , \qquad (21)$$

resembling the Fermi-Dirac function or hyperbolic tangent. The relevant value has been tabulated

	μ_{max} (cm² V⁻¹ s⁻¹)	μ_{min} (cm² V⁻¹ s⁻¹)	α	N_0 (cm⁻³)
Electron	1330	65	0.72	8.5 x10¹⁶
Hole	495	47.7	0.76	6.3 x 10¹⁶

The saturation of electron and hole drift velocity with the external electric field has also been discussed in Ref. [69]. The following formula

$$v_d = v_m \frac{E/E_c}{\left[1 + (E/E_c)^\beta\right]^{1/\beta}}, \qquad (22)$$

can fit experiments very nicely with the parameters summarized below.

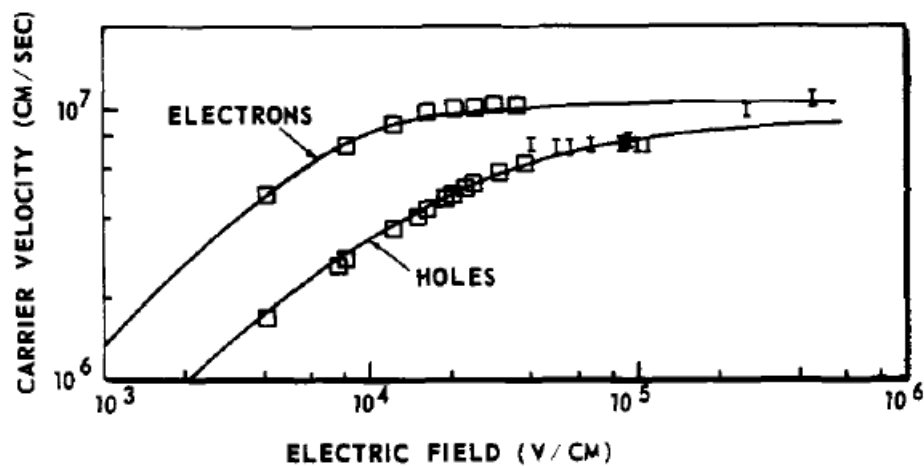|	v_m (cm/s)	E_c (V/cm)	β
Electrons	1.1 x 10⁷	8 x 10³	2
Holes	9.5 x10⁶	1.95 x 10⁴	1

Figure 13. Carrier-velocity as a function of electric field strength in silicon. [69]

Saturated drift velocity as in Figure 13 is common. A comparison of saturated drift velocity of semiconductors and breakdown electric field,[70]

Material	Diamond	Si	GaAs	SiC
Saturated drift velocity (10^7 cm/s)	2.7	1.0	2.0	2.7
Breakdown field (10^5 V/cm)	100	3	4	30

Semiconductor	Electron mass (m^*/m_e)	Electron mobility $(cm^2\ V^{-1}\ s^{-1})$	Hole effective mass (m_{hh}^*/m_e)	Hole mobility $(cm^2\ V^{-1}\ s^{-1})$
Si	0.98	1360	0.49	460
GaP	0.82	110	0.60	70
InP	0.08	4600	0.56	150
AlP	0.83	60	0.70	450
Ge	1.64	3900	0.28	1900
α-SiC		400		50
AlAs	0.146	200	0.76	100
GaAs	0.067	8500	0.45	400
InAs	0.022	33000	0.40	450
Al$_{0.48}$In$_{0.52}$As	0.083	4600	_	_

[70] E. F. Schubert, RPI (2003).

Ga$_{0.47}$In$_{0.53}$As	0.041	13800	0.50	350
InSb		5.25 x10^5 [71]		
Ga$_x$In$_{(1-x)}$Sb		1-5 x 10^4		400 - 1000
GaSb		5500 [72]		
AlN	0.40	300	3.53	14
GaN	0.20	1800	0.80	30
InN	0.11	3200	1.63	_

[71] Madelung, O.: Physics of III-V Compounds, J. Wiley & Sons, New York 1964; Collaboration: Authors and Editors of the LB Volumes III/17A-22A-41A1b: Indium antimonide (InSb), electron mobility. Madelung, O., Rössler, U., Schulz, M. (ed.). SpringerMaterials - The Landolt-Börnstein Database (http://www.springermaterials.com). DOI: 10.1007/10832182_388

[72] P. Damayanthi et al, Electron mobility and drift velocity calculations for bulk GaSb material, J. Appl. Phys. 86 (1999) 5060.

Table. A comparison of electron and hole mobilities in various III–V compound semiconductors at 300 °K. Data compiled by E. F. Schubert [73] and others. Si, Ge, and SiC data is also shown for comparison.

Semiconductor	Electron mass (m^*/m_e)	Electron mobility $(cm^2 \ V^{-1} \ s^{-1})$	Hole effective mass (m_{hh}^*/m_e)	Hole mobility $(cm^2 \ V^{-1} \ s^{-1})$
CdS	0.165	240-330 [74]	0.180	
CdSe	0.131	750 [74]	0.142	75
CdTe	0.111	1020 [75]	0.117	60
ZnS	0.230	80 - 200	0.254	10 - 15
ZnSe	0.180	260 - 560	0.193	5 - 38
ZnTe	0.151	330 - 1500	0.159	52 - 340

Table. A comparison of electron and hole mobilities at 300 °K in various binary II-VI compound semiconductors. Data compiled by R. L. Rode [75] and others.

Electron and hole mobility also depend on the semiconductor temperature.[75] This provides an option to operate detectors at lower temperature, which can reduce the detector noise and reduce detector response time significantly. For example, GaAs has a room temperature electron mobility of 7900 cm^2/V s. At 77 K, the mobility increases to 2.0 x 10^5 cm^2/V s.

[73] E. F. Schubert, http://homepages.rpi.edu/~schubert/.

[74] Data from Madelung, O., Rössler, U., Schulz, M. (ed.). SpringerMaterials - The Landolt-Börnstein Database (http://www.springermaterials.com). DOI: 10.1007/10681719_605.

[75] D. L. Rode, *Electron Mobility in II-VI Semiconductors,* Phys. Rev. B **2** (1970) 4036; Rode, D. L.: in "Semiconductors and Semimetals", Vol. 10. R. K. Willardson, A. C. Beer (eds.), Academic Press, New York 1975, p. 1.
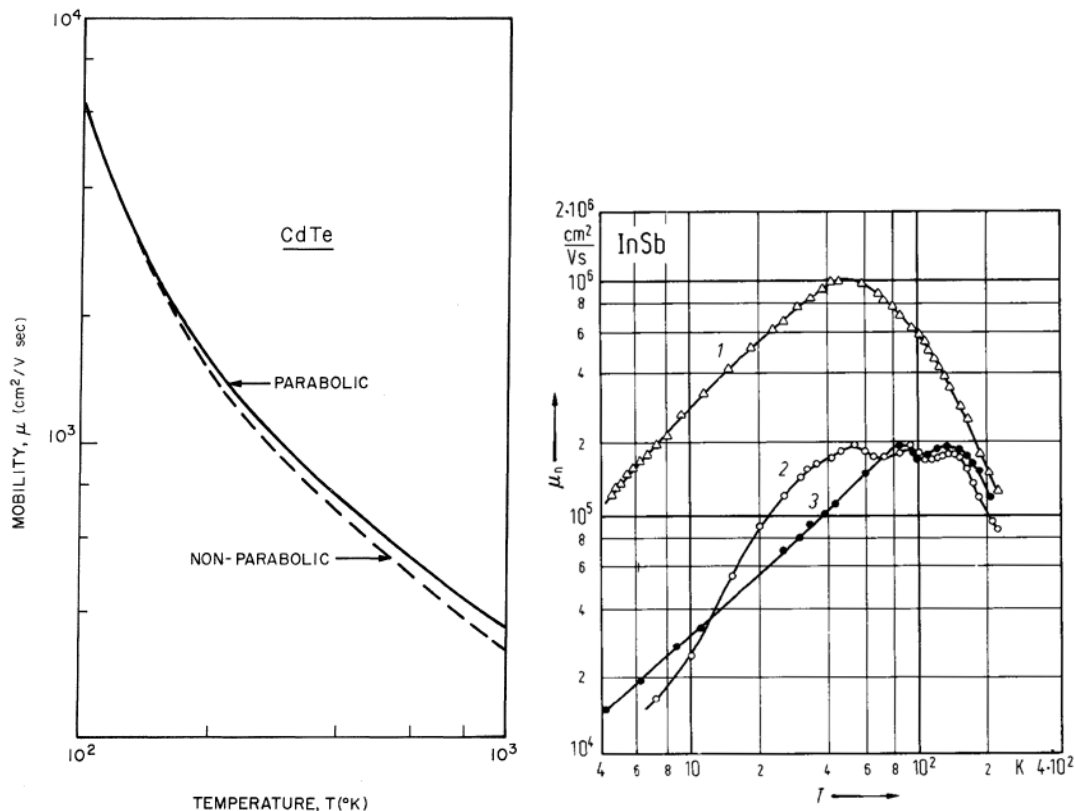
Figure 14. (Left) Electron mobility in CdTe calculated for a parabolc conduction-band valley and compared to that for the corrected nonparabolic band. The parabolic model predicts a higher mobility is in error by 15% at 500 ºK. [75] (Right) InSb. Electron mobility vs. temperature. Curve 1: pure material, curves 2, 3: impurity concentration > 10^{14} cm^{-3}.[76]

It is beyond the scope of this survey to discuss the large number of possible semicoductors for hard X-ray detection. Figure below includes some additional high-Z semicoductors of potential interest.

[76] Trifonov, V. J., Yaremenko, N. U.: Sov. Phys. Semicond. (English Transl.) 5 (1971) 839; Fiz. Tekh. Poluprovodn. 5 (1971) 953.

Figure 15. The band gap of typical IV-VI materials as a function of the lattice periodicity length (upper abscissa) or of the r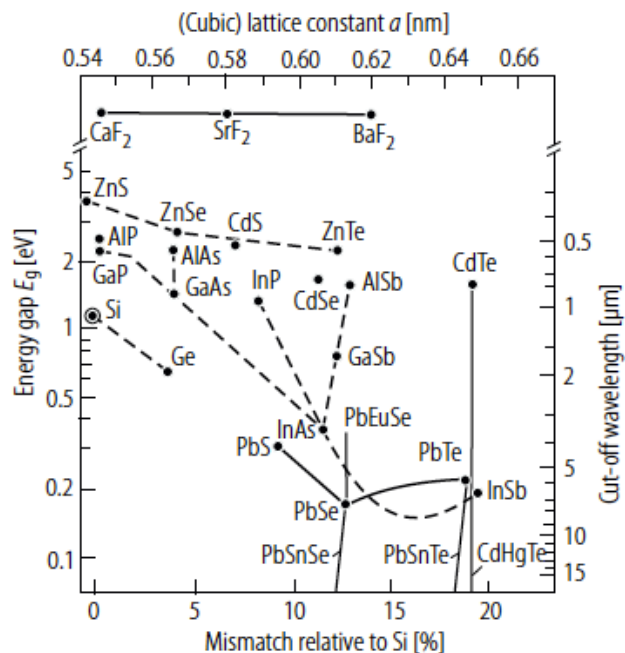elative lattice misfit to Si (lower abscissa). Si, Ge and some III-V and II-VI compounds are shown for comparison.[77]

It is useful to estimate the characteristic time for charge collection in different semiconductors. This time, defined as

$$\tau_{dr} = \frac{L_c}{\mu_{dr}E_0} = \frac{\ln 2}{n\sigma\mu_{dr}E_0}, \tag{23}$$

corresponds to the time for electrons drifting across a length $L_c = ln2/n\sigma$. μ_{dr} is the electron drift mobility, E_0 the applied electric field across the semiconductor. Using the X-ray absorption cross sections at 10 keV and 50 keV, L_c corresponds to the thickness of 50% X-ray absorption, one can plot τ_{dr} vs L_c, as in Figure 16 for 10 keV X-rays and Figure 17 for 50 keV X-rays. In both Figure 16 and Figure 17, room temperature is assumed and E_0 = 1000 V/cm. Therefore tens of ps charge collection time is feasible using InAs, GaInSb (Ga 50% and In 50%) and InSb. For 50 keV X-rays, the semiconductor are significantly thicker for 50% absorption efficiency, resulting in longer charge collection time and slower detector response time. Only InSb can deliver a charge collection time shorter than 100 ps. InAs and GaInSb take hundreds of ps for collection time. Therefore, it may require the detectors to operate at cryogenic temperatures and higher electric field to increase electron mobility and to achieve the as fast time response as possible for MPDH. The ultimate time response may be limited to

---

[77] M. Tacke, A. Ishida, *7 IV-VI Semiconductors*. Klingshirn, C. (ed.). SpringerMaterials - The Landolt-Börnstein Database (http://www.springermaterials.com). DOI: 10.1007/10479578_39; Zogg, H., Maissen, C., Blunier, S., Theodoropol, S., Overhsy, R.M., Richmond, T., Tomm, J.W.: Semicond. Sci. Technol. **8** (1993) 337.

saturated drift velocities in normal semiconductors. For an electron drift velocity of 1.0 x10^8 cm/s, the kinetic energy of the electron is 2.84 eV. At 5.2 x10^8 cm/s, which is assumed for InSb in FIGURE 16 and FIGURE 17, the drift kinetic energy is 77 eV. In other words, the electron motion is no longer in the drift regime but rather in the so-called ballistic transport regime. There have been numerous attempts in the past to build transistors based on this principle without much success. Nevertheless, new materials and structures, such as carbon nanotubes and graphene, offer new possibilities.
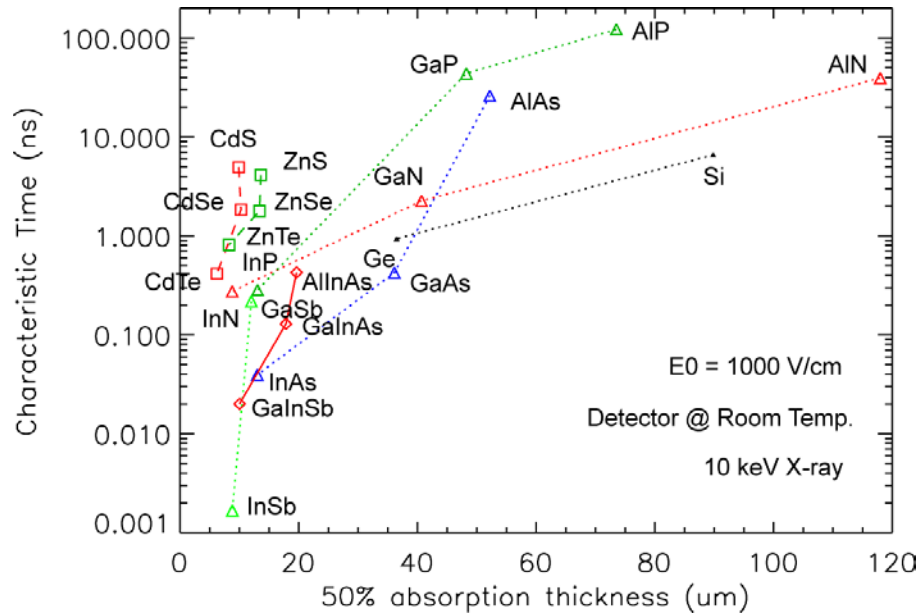

Figure 16. The projected electron drift time for various semiconductors after absorption of 10 keV photons. InAs, GaInSb, and InSb have charge collection time less than 100 ps for 50% X-ray absorption efficiency. Room temperature operation of the detectors is also feasible.
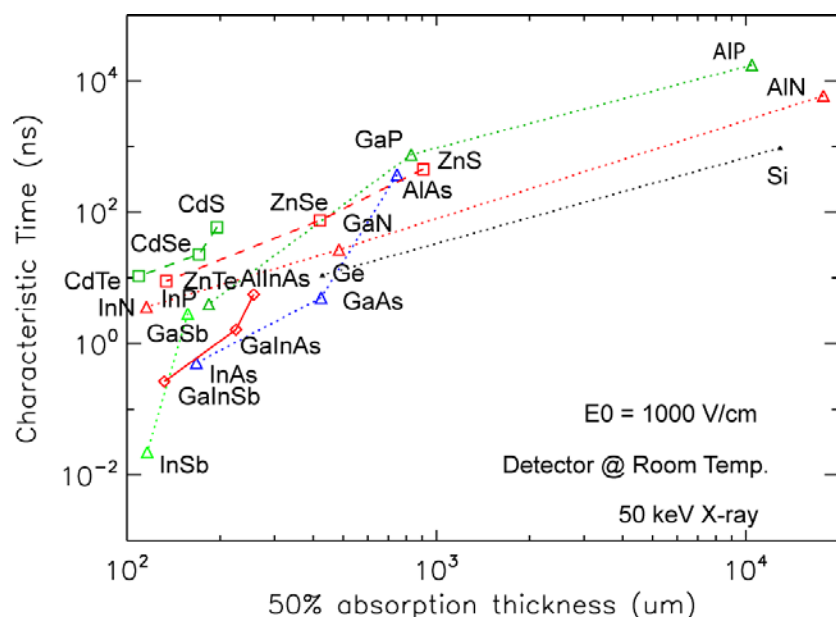
Figure 17. The projected electron drift time for various semiconductors after absorption of 50 keV photons. None of the surveyed semiconductor has charge collection time shorter than 100 ps for 50% X-ray absorption efficiency. Lowering the detector temperature and further increase in external electric field are possible ways to further increase electron drift velocity and therefore reducing charge collection time.

Photomultipliers, Photodiodes and Microchannel plates (MCP)

An extensive discussion on photomultipliers can be found in Knoll[15] and other standard references for radiation detectors, therefore no detail is given here.

A photodiode converts light to electric charge. Avalanche photodiode (APD) can be regarded as the semiconductor analog to photomultipliers. Compared with photodiodes, some of the advantages of APD include their compactness, high photo-electric efficiency (up to ~70%) for visible and infrared light. The response time of an APD can be as short as a few hundred (~ 300) ps.

A microchannel plate (MCP) is an array of 10^4 -10^7 miniature electron multipliers oriented parallel to one another.[78] Typical channel diameters are in the range of 10 to 100 μm and have length to diameter ratio between 40 to 100. Channel axes are typically normal to, or biased at a small angle (~ 8°) to the MCP input surface. The channel matrix is usually fabricated from a lead glass, treated in such as a way as to optimize the secondary emission characteristics of each channel and to render the channel walls semiconducting so as to allow charge replenishment from an external voltage source. Each channel can be considered to be a continuous dynode structure which acts as its own dynode resistor chain. Parallel electrical contact at each channel is provided by the deposition of metallic coating on the front and rear surfaces of the MCP, which then serve as input and output electrodes, respectively. The total resistance between electrodes is on the order of 10^9 Ohm. MCPs, used singly or in a cascade, allow electron

---

[78] J. L. Wiza, *Microchannel Plate Detectors,* NIM A **162** (1979) 587-601.

multiplication by a factor of 10^4 and 10^7 and coupled with <100 ps time resolution. The field of view is limited by the size of MCP. The spatial resolution is limited by the spacing from channel to channel. 12 μm channel diameter with 15 μm center-to-center spacings are typical. MCPs have direct sensitivity to charged particles, UV and X-ray photons.

Tremsin et al.[79] described a high resolution electron/photon/ion imaging system based on MCP that detects events with a timing accuracy of < 160 ps FWHM and a two-dimensional spatial accuracy of ~ 50 μm FWHM. The event counting detector used MCP for signal amplification and can sustain counting rates exceeding 1.5MHz for evenly distributed events (0.4MHz with 10% dead time for randomly distributed events)

The enhancement of the MCP dynamic range is possible by reducing MCP resistance. The negative temperature coefficient of the MCP resistance results in its thermal instability and therefore sets a lower limit to the resistance. To prevent thermal runaway, cooling of very low-resistance plates may be necessary.

Streak cameras

In terms of time response and temporal resolution, X-ray streak cameras can deliver a time resolution of a few hundred fs.[80] In comparison, the state of the art for optical streak cameras of 300 to 500 fs was reached in the late 1980s.[81] The quantum efficiencies of a streak camera are usually in the 0.1 to 10% range, mainly determined by the photocathode.[82] Commercial sources of streak cameras include Hamamatsu, Photonis, Optronis and Kentech.

CCD cameras

Boyle and Smith invented charge-coupled device (CCD) in 1969, for which they were awarded the Nobel Prize for Physics in 2009. One of the recent reviews on CCD's for X-rays can be found in [57]. CCD cameras themselves are not sufficient in general to detect hard X-rays directly. They belong to the Recording and Readout block as shown in Figure 8 and therefore need to be coupled with X-ray converters (phosphors, scintillators, or semiconductors) and signal amplifiers for effect X-ray detection. The intrinsic spatial resolution of CCD cameras, determined by pixel size of a few microns, does not necessarily apply to X-ray detection because of long stopping distances of hard X-rays. Lenses and fiber optical tapers are used to improve the spatial resolution for X-ray detection.

[79] A. S. Tremsin *et al. High spatial and temporal resolution photon/electron counting detector for synchrotron radiation research,* NIMA **580** (2007) 853.

[80] V. Pitre et al. *Characterization of the new FX1 x-ray streak camera,* in Proc. SPIE **5194** (2004) 115.

[81] K. Kinoshita, M. Ito, and Y. Suzuki, "*Femtosecond streak tube,*"Rev. Sci. Instrum. **58** (1987) 93; H.-B. Niu, et al., *Theoretical and experimental study of femtosecond streak image tube,*"in 18th Intern. Congr. High Speed Photography and Photonics, edited by D.-H. Wang, Vol. **1032** (1989) 472; A. Finch, et al., Development and evaluation of a new femtosecond streak camera," *ibid.* 622.

[82] J. Liu, J. Wang, B. Shan, C. Wang, and Z. Chang, "An accumulative x-ray streak camera with sub-600-fs temporal resolution and 50-fs timing jitter," Appl. Phys. Lett. **82** (2003) 3553–3555.

Based on light-collection schemes, there are two types of CCDs: front-illuminated (FI) CCDs and back-illuminated (BI) CCDs. In an FI CCD, an X-ray photon has to pass through the gate before absorption. In a BI CCD, an X-ray photon enters the absorption regime without having to pass through the gate. BI CCDs normally have a higher detection quantum efficiency (QE) for low-energy X-rays than that of FI CCD, see Figure 18 and Figure 19. FI CCDs were developed earlier than the BI CCDs.
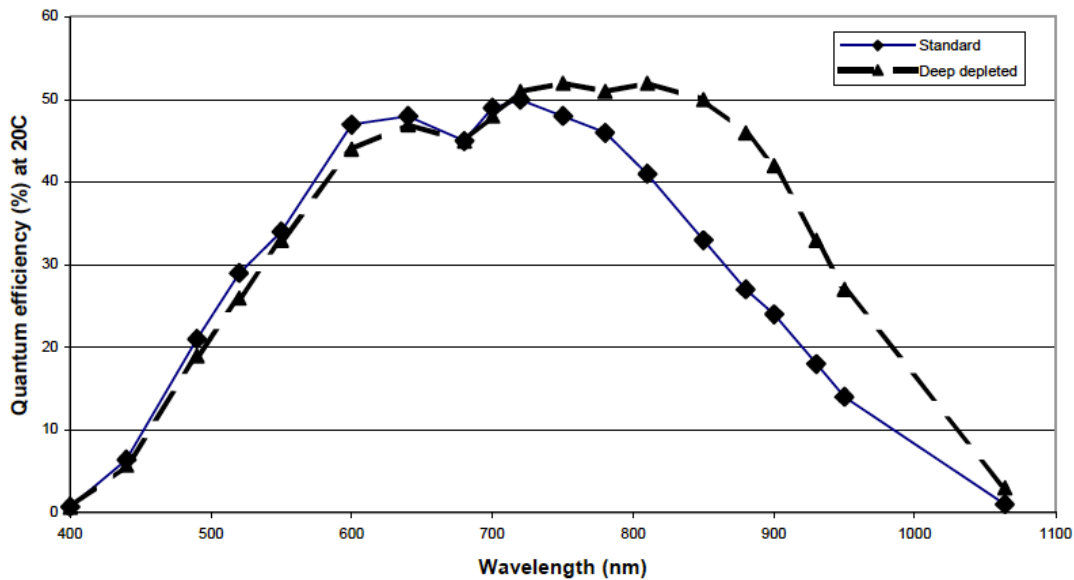
Figure 18. Typical quantum efficiencies of front-side illuminated CCD- comparison of standard and deep-depletion silicon response.[83]

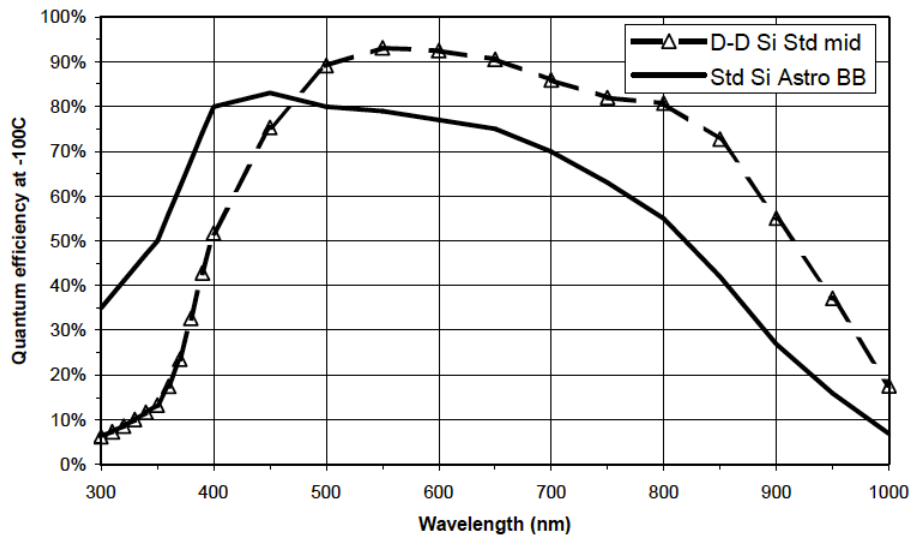**Figure 19. Quantum efficiencies of Backside illuminated CCD- comparison of standard and deep depletion silicon (note that different AR coatings have been applied in the two cases). The data is also from e2V as in Figure 18.**

---

[83] Data from http://www.e2v.com/products-and-services/high-performance-imaging-solutions/technical-papers/.

The architecture of a CCD camera is shown schematically in Figure 20. Online sources provide more visual illustration about CCD structures and their operating principles.[84]
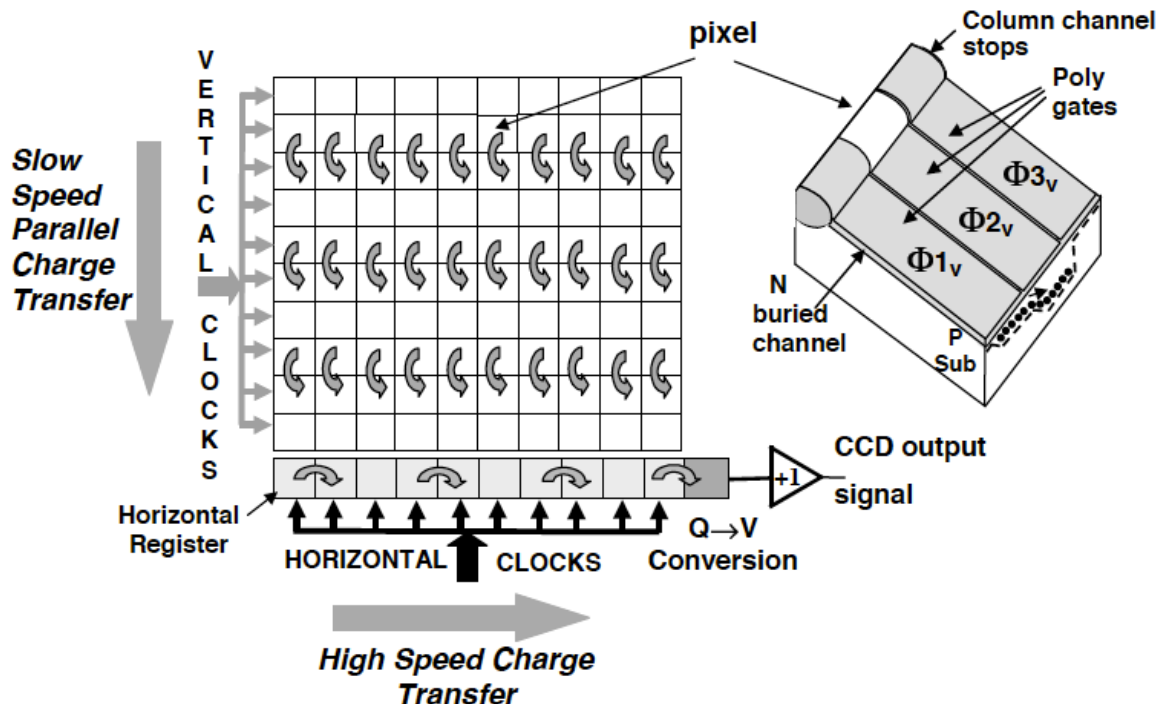
Figure 20. An example of a CCD architecture.[85]

Many X-ray CCD cameras exist commercially. For example, Princeton Instruments/Roper Scientific makes PIXIS-series X-ray cameras, Andor makes iKon-L X-ray CCD camera and others.[86] There are also intensified CCD cameras (ICCD). An advantage of the gateable ICCD cameras is their ability of ultrafast gating. Shutter speeds, i.e. exposure times of 5 to 10 ns, are typical with gateable ICCD cameras. Standford computer optics[87] can gate at a speed of about 260 ps at 1% opening.

An off-the-shelf X-ray CCD camera selection guide is shown below.[88] However, most of the off-the-shelf CCD cameras would not be useful for MPDH, due to their low efficiencies for hard X-rays above 10 keV in energy, and in particular very slow frame rate on the order of 100 fps.

---

[84] See for example, http://www.specinst.com/What_Is_A_CCD.html.

[85] P. Magnan, *Detection of visible photons in CCD and CMOS: a comparative view,* NIM A **504** (2003) 199-212.

[86] http://www.andor.com/scientific_cameras/x-ray/.

[87] http://www.stanfordcomputeroptics.com/t-shutter.html.

[88] Based on a brochure published by Hamamatsu.
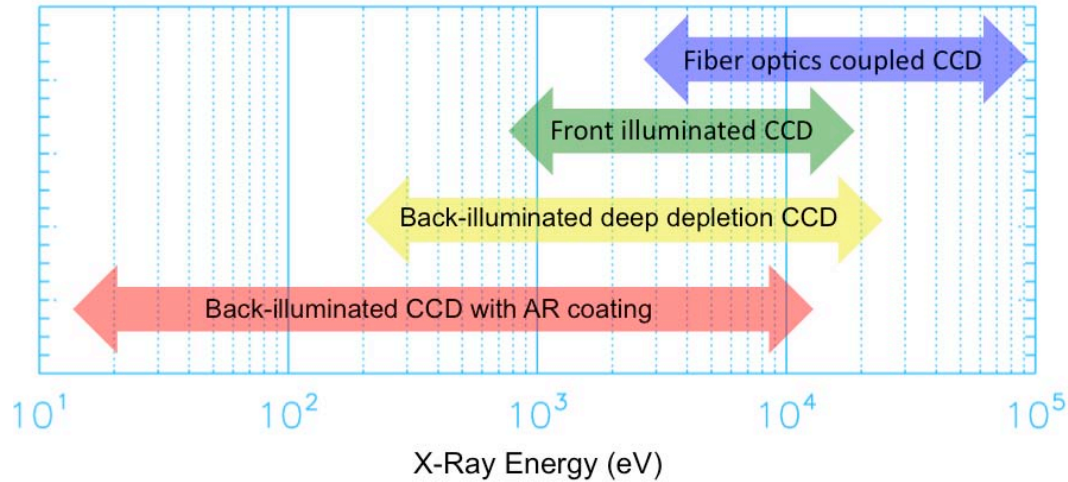
Figure 21. An X-ray CCD camera selection guide for imaging. Most of these cameras would not be useful to MPDH dynamic experiments.

CMOS cameras

Historically, CMOS technology for imaging was developed later than CCD technology. Advance of CMOS fabrication technology is describable by Moore's law.[89] The current state-of-the-art is at so-called deep submicron (L < 0.25 μm) scale for MOSFET channel length. Each pixel of a CMOS camera is a mini-detector that combines light detection, charge-to-voltage conversion and transistors providing buffering and addressing capability. This memory-like organization, in contrast to CCD architecture, provides random access to individual pixels and direct windowing capability at a high frame rate and avoids the multiple charge transfers over long distances of the CCD architecture that are very sensitive to radiation degradation.[85]

---

[89] A. S. Sedra and K. C. Smith, *Microelectronic Circuits, 6th Ed.* (Oxford University Press, New York, London, 2010), p.1122.
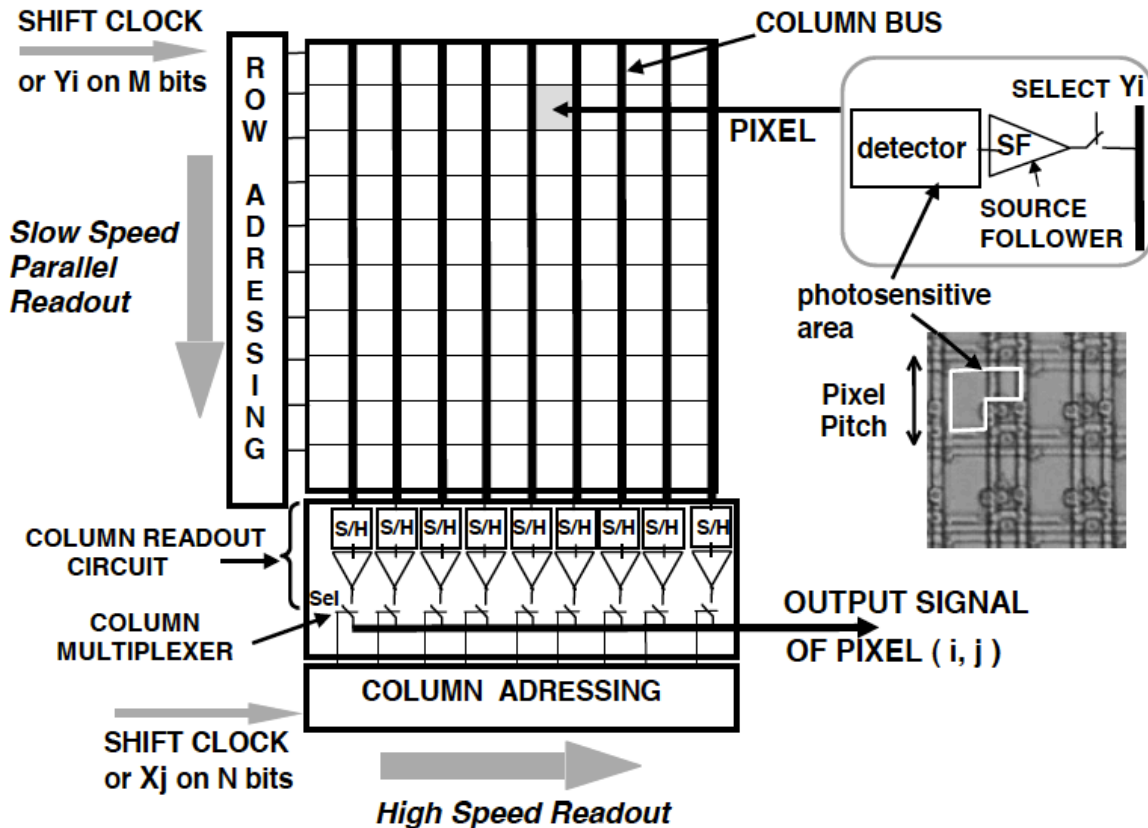
Figure 22. CMOS architecture, from the same reference as in Figure 20.

In terms of photon sensitivity, the PILATUS X-ray detectors,[90] which are based on the CMOS hybrid-pixel technology, can operate in single-photon-counting mode with a dynamic range of 20 bits. The existing upper detection limit of 40 keV X-ray energy would have to be increased for MPDH X-ray by, for example, increasing the thickness of the silicon sensor.
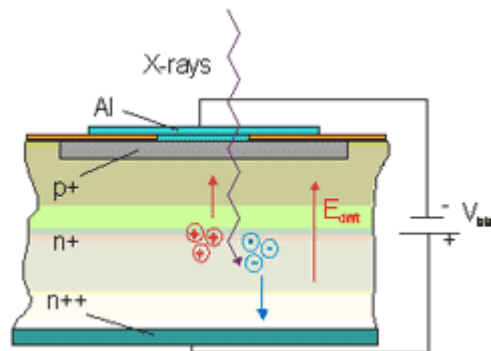
Figure 23. . Operating principle of a PILATUS detector. An X-ray photon is directly transformed into electric charge in a 0.32 mm thick silicon sensor and processed in CMOS readout chips.

---

[90] http://www.dectris.com.

An evolution of hybrid CMOS image sensor technology at Teledyn is shown below.[91] Other manufacturers follow similar trend.
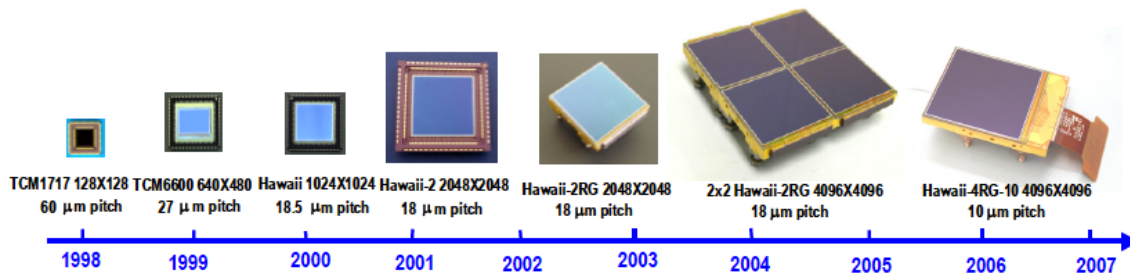
4.2. Detector lifetime

Detector lifetime is limited by radiation damage to the detector, resulting in degradation of malfunctions of its components, the front end and the readout electronics in particular. Every x-ray imaging application is unique and detector lifetime needs to be looked up based on the construction of the detector as well as the radiation environment. Radiation dose can be calculated quite accurately (see below), while the detector lifetime depends on a quite number of random events. Therefore, detector lifetime should be measured experimentally. In terms of damage mechanism, X-rays do not affect the crystal structure or atomic order of the detector material, but they can produce a large number of free electrons, and about the same number of positively charged ions (or holes). If the material is conductive, the electrons can quickly recombine, and the crystalline structure of the material is restored. However, if the material is an insulator, the energetic electrons often get ejected, leaving behind a permanent positive charge that can modify the behaviors of charge transport in a later time.

Integrated circuits rely on one or more insulating or dielectric layers to separate conductors and help control electric fields inside the device.[92] Both CCDs and CMOS devices employ a thin layer of silicon dioxide (SiO_2) to separate polysilicon electrodes from the bulk silicon underneath. Charge build-up in this SiO2 layer directly modifies the underlying electric fields, and therefore the charge transport properties of the silicon. In a CCD this means that the charge transfer becomes inefficient and the device quickly stops working. In a CMOS transistor it means that the threshold voltage of the transistor slowly shifts, until the device is either always on or completely closed off. Digital devices, as well as carefully designed analog devices, are able to tolerate moderate amounts of threshold voltage shifts, enabling them to continue to function normally until the transistors stop working and the device fails. The charge distributions and electric fields at the perimeter of the photodiode, where the depletion region intersects

---

[91] Y. Bai et al., Teledyne Imaging Sensors: Silicon CMOS imaging technologies for x-ray, UV, visible and near infrared, Proc. SPIE Conf. Astron. Instrum. (2008, Marseille, France)
[92] Rad-icon Imaging Corp AN06: Detector Lifetime and Radiation Damage.

with the device surface, are very sensitive to disturbances. Positive charge in the oxide layer causes electrons to accumulate underneath the surface, modifying the charge density in the depletion region and thereby increasing the leakage current across the PN junction of the diode. The dark current becomes stronger with increasing absorbed dose, until the diode eventually discharges faster than it can be read out.

In a CMOS imaging sensor the most visible effect of radiation on device performance is seen in the dark current. Long before the transistors in such a device show any sign of change in behavior, the dark current from the photodiodes begins to increase. Modern CMOS sensors like the RadEye1 image sensor start off with extremely low dark current – on the order of 25 pA/cm^2 – so that even a strong increase in dark current will not have a significant effect for quite a while. The physical mechanism responsible for the increasing dark current is the same buildup of positive charge in the oxide layer.

Radiation hardness

One can convert incident photon flux into required dose, which is defined as absorbed energy per unit mass,[27]

$$Dose = (\Gamma \Delta t)\mu E / \rho, \tag{24}$$

where $(\Gamma \Delta t)$ is the total number of photon flux per unit area, μ is the linear absorption coefficient, ρ is the mass density, and E is the X-ray energy.

Radiation hardness, a rough measure of the accumulated absorbed dose that causes a reduction of 1 to 2% in the optical transmittance per thickness of μ/ρ.

4.3. Detector Instruments in Major Synchrotron and XFEL facilities

The third generation of X-ray photon sources is based on synchrotron storage ring. The major facilities are 7-GeV Advanced Photon Source (APS) in the US, 6-GeV European Synchrotron Radiation Facility (ESRF) in France, and 8-GeV Super Photon Ring 8-GeV (SPring-8) in Japan. In the longer wavelength regime, which corresponds to lower electron energies, there are facilities like ALS (1.9 GeV), NSLS-II (3 GeV), and close to 100 other light sources around the globe.[93] There are plans and funded efforts to upgrade the existing sources. While storage ring technology continues to improve and further advances may be expected, the consensus in the accelerator physics community is that the technology is mature and at the point of diminishing returns.[94] It has also been noticed that as it takes longer and longer from the initial proposal to the final commission of a new facility, how to sustain the financial support is becoming a challenging issue for each of the major facilities.

---

[93] W. Namkung, *Review of third generation light sources,* Proceedings of IPAC'10, Kyoto, Japan.
[94] Ropert A, Filhol J M, Elleaume P, Farvacque L, Hardy L, Jacob J and Weinrich U, *Towards the ultimate storage ring-based light source* Proc. EPAC 2000 (2000) 83.

The fourth generation of X-ray photon sources is based on XFEL. The unique features of XFEL are emission of ~ 0.1 nm coherent hard X-ray photons at high peak power and short pulse length. XFEL relies on the so-called Self-Amplified Spontaneous Emission (SASE) principle for gain. SASE does not need cavities or mirrors, thus wavelength of an XFEL is continuously tunable. A table of major XFEL facilities is listed below. Other proposed facilities, such as NGLS, are not included.

Facility	e-beam	Wavelength (nm)	pulse	Photons per bunch	Brilliance
LCLS	14.3 GeV	0.15 – 1.5	230 fs, 8 -10 GW, 120 Hz		
FLASH	≤ 1 GeV	4.5-47	10-50 fs 0.15 - 4 MHz 1-5 GW	10^{12}-10^{13}	10^{29}-10^{30}
FLASH II	1.25 GeV	4 - 80	<70-200 fs 0.3 – 2.5 MHz 1-3 GW	10^{12}-10^{13}	10^{28}-10^{31}
European XFEL	10-20 GeV	0.1 - 3		10^{12}	
SCSS	2-8 GeV	0.08-6	500 fs 3 GW (for 0.1 nm) 60 Hz	7.6×10^{11} (for 0.1 nm)	

Extension of time-resolved X-ray diffraction to the sub-ps domain is an important challenge.[95] The current state-of-the-art detector for XFELs is the CAMP instrument and its pnCCD detector.[96] 1 Megapixel, ~6 e- low noise, 200 Hz readout. This has been used at end-stations at LCLS, certainly the soft x-ray AMO station.

LCLS detectors[97]

LCLS (The Linac Coherent Light Source) Ultrafast Science Instruments are collectively known as LUSI. LUSI comprises: The Coherent X-ray Imaging (CXI) Instrument, The X-ray Pump/Probe (XPP) Instrument, The Coherent X-ray

---

[95] C. Rischel et al*., Femtosecond time-resolved X-ray diffraction from laser-heated organic films,* Nature **390** (1997) 490.

[96] Struder, L ; Eppa, S ; Rolles, D ; Hartmann, R ; Holl, P ; et al., *"Large-format, high-speed, X-ray pnCCDs combined with electron and ion imaging spectrometers in a multipurpose chamber for experiments at 4th generation light sources,"* NIM A **614** (2010) p.483-496 and the many correlated references to this technology (appears perhaps to have been developed for x-ray satellites?).

[97] http://lcls.slac.stanford.edu

Scattering (CXS) Instrument and The X-ray Correlation Spectroscopy (XCS) Instrument. LUSI make use of the coherent X-ray photons in the wavelength range between 0.15 nm and 1.5 nm, or 830 eV to 8.3 keV in photon energy. The different instruments basically rely on three kinds of detectors.

CS-PAD camera,[98] a collaboration between SLAC and Cornell, is used or will be used in the XPP, CXI, and Matter in Extreme Conditions (MEC) hutches. The camera works with 8.3 keV photons. 110 mm x 110 mm x 500 μm thick pixels. Array of 758 x 758 pixels. Readout at 120 Hz using RCE-based DAQ. High and low gain modes. Bump-bonded, hybrid architecture. Dynamic range, for an 8 keV, the signal response is 10.5 ADUs. Full capacity in low gain mode is over 7000 8 keV photons. The noise is ~ 2.3 keV rms.

Figure 24. (left) the CS-PAD camera. (middle) A quarter of possible modules mounted. (right) Being installed on a XPP robot arm.

The harder-x-ray CXI instrument is a CS-Pad bump-bounded with ASICs under it. This is a mosaic system of many individual detectors. It generates 200 TBytes of data at 120 Hz running for a whole week. Anton Barty spoke about its use; off-line he said words like "two PAD detectors operating at 120 Hz at CXI at LCLS, should have 24 counts per ~9keV photon, but only getting ~8 with ~4 dark noise. Only able to see bright Bragg peaks." Nevertheless they at getting 2 - 4 Angstrom resolution single protein structure.

X-ray Active Matrix Pixel Sensors (XAMPS) detector,[99] a collaboration between SLAC and Brookhaven, is intended for uses in XPP and in XCS. XAMPS are based on J-FET technology and produced on 100 mm high-resistivity silicon, typically 400 μm-thick. The prototypes are square matrices with n rows and n columns with n = 16, 32, 64, 128, 256, 512. Each pixel of the matrix is 90 × 90 μm2 and contains a JFET switch to control the charge readout. The XAMPS is a position sensitive ionization detector. It consists of a pixel array detector with integrated switches. Pixels are isolated from each other by a potential barrier and the device is fully depleted by applying a high voltage bias to the junction on the entrance window of the sensor. The small features of the design presented some

---

[98] The name CS-PAD stands for Cornell Standford –PAD.

[99] G. A. Carini, W. Chen, A. Dragone et al., *Tests of small X-ray Active Matrix Pixel Sensor prototypes at the National Synchrotron Light Source,* J. Instrum. **4** (2009) P03014 doi:10.1088/1748-0221/4/03/P03014;

technological challenges fully addressed during this production. The first prototypes were tested at the National Synchrotron Light Source (NSLS) with a monochromatic beam of 8 keV and millisecond readout and exhibit good performances at room temperature.

XCS detector is a single stage CCD device, a collaboration between SLAC and BNL. The detector is intended to provide 100% DQE, 10^2 dynamic range, very low noise (<<1photon) 55x55 μm^2,1k x1k pixels,120 fps. An alternative is an Princeton Instrument LCX detector with a standard direct illumination CCD, which provides 50% DQE at 8keV (30% at 10 keV), 50 photon dynamic range, very low noise (<<1photon) 20x20 μm^2, 1.3k x 1.3 k pixels, and 0.3 fps.

FLASH detectors.[100]

pn-CCD. Conceptually the pn-CCD,[101] the heart of the MPE focal plane detector for XMM-Newton, is a derivative of the silicon drift detector proposed in 1983 by Gatti & Rehak (1984)[102]

For uses in the 3rd (FLASH) and 4th generation coherent X-ray sources such as LCLS and European XFEL, pn-CCDs come in various format sizes from 512 x 512 up to 2048 x 2048. A 1024 x 1024 format corresponds to a physical area of 80 x 80mm^2. With voxel dimensions of 75 x75 x 450 μm^3, more than 80% quantum efficiency can be achieved for X-rays with energies in the range from 0.3 to 12 keV.[96] A typical read-out noise is 2.5 electrons (rms) at an operating temperature of -50 ^{o}C. These detectors operate with a frame read-out rate up to 200 Hz. The pnCCD is fabricated on double-sided, polished, n-type 150 mm silicon wafers, typically 300–500 μm thick. Typical electric bias is approximately 0.5V/μm. The front-end electronics will be equipped with 16 ADCs running at 10 MHz each with a resolution of 14 bit. The data rate is 0.5 GB per second.

[100] http://hasylab.desy.de/instrumentation/detectors/index_eng.html.

[101] L. Struder et al., The European Photon Imaging Camera on XMM-Newton: The pn-CCD camera, A&A 365, L18{L26 (2001).

[102] E. Gatti and P. Rehak, NIM A **225** (1984) 608-621.
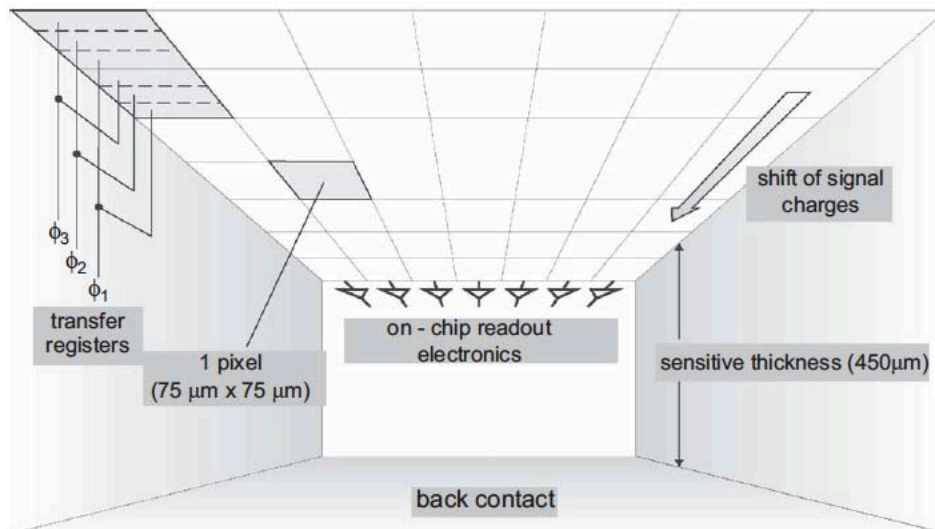
Figure 25. Schematic view from the inside of a pnCCD. More details can be found in [96].

Medipix3 Medipix was a hybrid pixel detector readout chip developed at CERN. The third generation of this chip, Medipix3, is currently being developed. Each pixel on a semiconductor sensor is bonded to a channel on the Medipix chip. The Medipix chip performs single photon counting, much like the Pilatus detector system; each X-ray hit on a pixel generates a signal pulse, and the pixel circuitry counts the number of hits over an adjustable energy threshold. This means that the detector can achieve single-photon sensitivity, and does not suffer from the "blooming" effects seen in integrating detectors like CCDs. Since the photons are directly converted to an electrical signal in the semiconductor, rather than relying on indirect conversion, the point spread function is small. The chip can also be read out at a high rate. Medipix3 will have small pixels (55μm), and will operate in a "continuous read-write" mode with very little dead time. Communication between adjacent pixels will reduce the effects of signal sharing, allowing the chip to distinguish between different photon energies more effectively – for example, to exclude fluorescence photons.

DESY is developing larger-area Medipix3 modules, incorporating 12 Medipix3 chips to give an array of 1536 by 512 pixels (28mm by 85mm). These modules are being designed to have a small edge region, so that they can be tiled to cover a larger area. A high-frame-rate readout system is also being designed, based on developments for XFEL. The Medipix3 chip and large-area module are designed to be compatible with a wide range of different materials, such as germanium, GaAs, and CdTe.

High-Z Detectors: Germanium Detector Project, Galapad (GaAs) and HiZPAD (CdTTe)

XNAP pixel detector

European XFEL detectors.

The European X-ray free electron laser is a new research facility currently under construction in Hamburg, Germany. Typical for XFEL machines is the high peak brilliance several orders of magnitudes above existing synchrotron facilities. With a pulse length below 100fs and an extremely high luminosity of 30,000 flashes per second. The European XFEL will have a world-wide unique time structure that enables researchers to record movies of ultrafast processes. This demands the development of new detectors tailored to the requirements imposed by the experiments while complying with the machine specific operation parameters.The *adaptive gain integrating pixel detector* (AGIPD) is one response to the need for large 2D detectors, able to cope with the 5MHz repetition rate, as well as with the high dynamic range needed by XFEL experiments (from single photons to 10^4 12 keV photons per pixel per pulse). In addition, doses up to 1GGy over three years are expected.[103]

The *Adaptive Gain Integrating Pixel Detector* (*AGIPD*) project[104] is a collaboration between DESY, PSI, University of Bonn, and University of Hamburg, established to develop and construct a detector with 1 million pixels, of 200 x 200 μm^2, based on the *hybrid pixel technology[105]*. Each pixel will contain an adaptive slope integrator needed to cover the full dynamic range from single photon detection up to 10^4 12 keV photons per 100 fs pulse, as well as an analog pipeline for frame storage at the 5 MHz repetition rate. Precautions will also be taken to make the detector sufficiently radiation hard, as the total integrated lifetime dose could exceed 1 GGy. A single ASIC will contain 64×64 pixels and be three side buttable, 4×2 ASICs will be bump-bonded to a monolithic 500 or 700 μm thick silicon sensor to form a module, and (4×8) modules will be assembled to form the complete 1K x 1K pixel detector. In order to allow the direct beam as well as the forward scattered sample signal to pass without damaging the detector, a hole is present at the center of the detector. The readout of the analog pipeline and digital conversion will be done during the 99.4 ms time gap between bunch trains. As many pictures as possible, at least several hundred, will be stored in the ASIC during the bunch train. The exact number will be determined as a compromise between various conflicting parameters like noise versus number of storage capacitors.

The new DSSC (DEPFET sensor with signal compression) detector system[106] is being developed in order to fulfil the requirements of the future XFEL in Hamburg. The instrument will be able to record X-ray images with a maximum frame rate of 5 MHz and to achieve a high dynamic range. The system is based

[103] B. Henrich, J.Becker, R.Dinapoli, et al, *The adaptive gain integrating pixel detector (AGIPD), a detector for the European XFEL*, NIM A **633** (2011) S11-S14.

[104] G. Potdevin, U. Trunk, H. Graafsma and For the AGIPD Consortium, *Performance simulation of a detector for 4th generation photon sources: The AGIPD*, NIM A **607** (2009) 51-54.

[105] H. Spieler, *Semiconductor Detector Systems*, Oxford Science Publications, 2008.

[106] M. Porro, L. Andricek, L.Bombelli, et al, *Expected performance of the DEPFET sensor with signal compression: A large format X-ray imager with mega-frame readout capability for the European XFEL,* NIM A **624** (2010) 509-519.

on a silicon pixel sensor with a new designed non-linear-DEPFET as a central amplifier structure. The detector chip is bump-bonded to mixed signal readout ASICs that provide full parallel readout and temporary data storage. The signals coming from the detector are processed by an analog filter, immediately digitized by 8-ENOBADCs and locally stored in accustom designed memory. The ASICs are designed in 130 nm CMOS technology. During the time gap of 99 ms of the XFEL machine, the digital data are sent off the focal plane to a DAQ electronics that acts as an interface to the back-end of the whole instrument. The pixel sensor has been designed so as to combine high energy resolution at low signal charge with high dynamic range.This has been motivated by the desire to be able to be sensitive to single low energy photons and, at the same time, to measure at other positions of the detector signals corresponding to up to 10^4 photons of 1 keV. In order to fit this dynamic range into a reasonable output signal swing, achieving at the same time single photon resolution, a strongly non-linear characteristic is required. The new proposed DEPFET provides the required dynamic range compression at the sensor level, considerably facilitating the task of the electronics. At the same time the DEPFET charge handling capacitance is enormously increased with respect to standard DEPFETs. The sensor matrix will comprise 1024x1024 pixels of hexagonal shape with a side-length of 136 mm. The simultaneous implementation of the 5 MHz frame rate, of the single low-energy photon resolution and of the high dynamic range goes beyond all the existing instruments and requires the development of new concepts and technologies.

SCSS detectors.[107]

 SPring8 Compact SASE Source (SCSS) in Harima, Japan has similar parameters to LCLS and a repetition rate of 60Hz.

4.4. A detector classification scheme

There are ten to one hundred kinds of X-ray detector and systems to serve broad functions of medical diagnosis, non-invasive scanning and fundamental sciences. These detectors use different material for X-ray capture, employ unique engineering architectures for real-time signal processing and on-board data storage. The family of X-ray detectors is only expected to grow. The performance of an X-ray detector is measured by more than ten parameters. In terms of detector functions, there are imaging devices (various types of CCD cameras, CMOS cameras), photon counting devices (Medipix, Pilatus, XPAD, Eiger), signal integrating devices (similar to detectors used in HEP, such as ATLAS, CMS, CS-PAD, 3DX, AGIPD, DSSC), and timing devices (streak cameras, Timpix). In terms of material usage, there can be scintillating devices, semiconductor devices, liquid devices, gas detectors and even plasma devices. In terms of In terms of engineering details, there can be nano-devices, micro-devices, and traditional macro-devices.

---

[107] see http://www-xfel.spring8.or.jp

Sometimes, a condensed comparison of different detector schemes can be quite useful. For example, the following table is produced based on a scheme for visible light.[108]

	PMT	Film	CCD	CMOS
Dynamic range	>1000	<100	>10,000	>5,000
Detection speed	ns	not real-time	ms	μs
QE[109]	5-20%	<1%	>50%	>50%
Format	$< 10^2$	$>1000^2$	$>1000^2$	$>1000^2$
Dark signal	good	poor	best	best
Read noise	good	good	best	best

To identify the research needs for MPDH, a more detailed and quantitative parameter set is generated here. At the present, no single detector system meets all the functional requirements of MPDH simultaneously. The largest gaps are highlighted.

Parameters	MaRIE values	Relevant existing technology
Photocathode (equivalent Z)	InSb or higher	Si, CdTe, NaI, CsI
Energy Range	50-100 keV	1 - >100 keV[110]
Energy resolution @10 keV (Spectral resolution)	< 400 eV	<400 eV
Readout noise	< 1 e^-	< 10 e^-
DQE @10 keV	> 50%	> 50%
DQE @ 50 keV	> 50%	< 20%
Gain @10 keV	1 - 50	1 - 50
Dynamic range	≥ 20 bit	14 – 31 bit

[108] Similar to Table from http://www.specinst.com/What_Is_A_CCD.html.
[109] X-ray photon energy dependent. We use 10 keV as reference, since they are more common at this point.
[110] For imaging sensors.

Pixel size	50 to 3000 μm	30 to 3000 μm
Format size	1000 x 1000	7000 x 7000
Gating time	1 ps	300 ps
Frame rate	3-10 GHz	~ 1 MHz
Number of frames	20-10000	~10
Detector temperature	≤ 300 K	≤ 300 K
Fill Factor	> 90%	> 90%
Useful life time (hours)	> 100 hours	> 100 hours

Terminology[111]

ADC resolution or *Bit depth*. Bit depth is specified in base 2 notation. Eight bits is 2^8 or 2 raised to the 8th power. Eight bits equals 256 steps or levels of information. Twelve bits is 2^{12} and equals 4096 levels. Sixteen bits is is 2^{16} and equals 65,536 levels.

ADU Analog to digital unit. A number that represents the CCD or CMOS imaging sensor's digital output. The number of electrons in each ADU is determined by the system gain.

Array format Also known as *pixel resolution*.

ASIC Application specific integrated circuit

ATCA a communication and packaging standard developed and maintained by the PCI Industrial Computer Manufacturers Group (PICMG)

Bit depth See *ADC resolution*

Blooming Electrons that spill over into adjacent wells when a potential well is full cause blooming, which appears as vertical spikes from bright stars that are overexposed.

Bump Bond A technique/procedure to integrate detector array with readout array.

Charge capacity see *full well capacity*

CMOS complimentary metal oxide semiconductor

Dark current Also known as thermal current. Signal that is generated by electron and hole pairs created in the silicon substrate of a CCD or CMOS sensor by heat. Dark current increases as temperature goes up. Dark current happens even without exposure to light, hence the name "dark current". Defects in the

---

[111] Some additional terminology can be found, for example, at
http://www.astropix.com/HTML/I_ASTROP/GLOSSARY.HTM.

bulk silicon or other semiconductors and at the surface will cause an excessive amount of dark current. 5-10 nA/cm^2 (298K) is normal.

Dark (Thermal) Current Noise Noise that is generated because of statistical variations in thermal (dark) current, equal to the square root of the thermal current. Because it is random, it cannot be removed from an image.

DQE Detective Quantum Efficiency

DQE^2

DR digital radiography

Dynamic range sometimes expressed in dB.

Fill Factor

Fill Factor and Pixel Resolution
produce superior images with CMOS

Amorphous Silicon
127 micron pixels

CMOS
80 micron pixels

1/4 mm (0.010 inch)

63% fill factor

92% fill factor

Fill factor means the portion of the detector that is active sensor
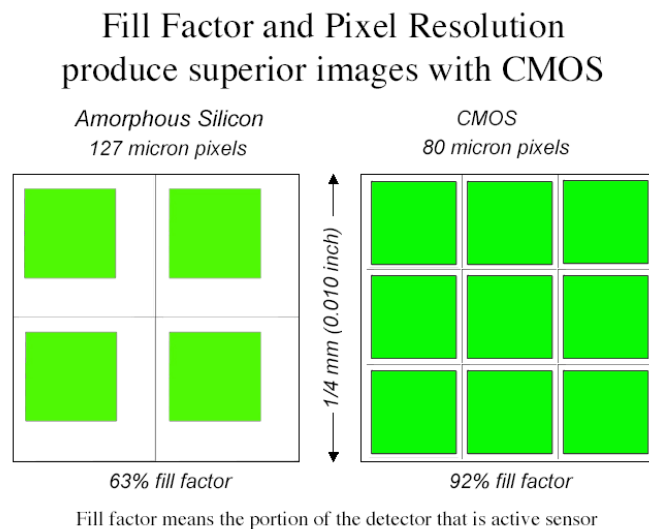
Form factor 1kx1k

Format size See *Form factor*

FPA Focal plane array

Frame rate 900 Hz frame rate, in frames per sec (fps) or Hz.

Full well capacity measured in the number of electrons, such as 9000 e$^-$.

Image blooming See *blooming*

Image Lag the presence of residual image information in successive images, that is typical of amorphous thin-film transistors (TFT) technologies.

Latent Image Image data "left-over" from a previous exposure showing up in a later image.

MTF modulation transfer function. MTF is a measure of spatial resolution. An MTF closer to 1.0 implies the image looks more like the object.

NPS Noise power spectrum

Number of outputs for each pixel, can be 1, 4, 16, 32 or 64

PIN p-type, intrinsic, n-type

Pixel amplifier different types include source follower (SF), Direction injection (DI) and capacitive transimpedance amplifier (CTIA).

Pixel binning 1x1, 1x2, 1x4, 2x1, 2x2, 2x4, 4x1, 4x2, 4x4

Pixel pitch measured in micrometer, such as 27 μm

Pixel rate in MHz range

Pixel Resolution 1280 x 1280, 7680 x 7680

Power dissipation Usually measured in mW. Normally < 100, can be a few thousand.

QE 65% peak, lower in blue & red.

Readout mode different modes include Snapshot, Ripple.

RCE Reconfigurable Cluster Element[112]

RCE is a generic computational building block based on *System-On-Chip* (SOC) technology capable of operating from 1 to 24 lanes of generic high-speed serial I/O. These lanes may operate individually or bound together and may be configured to operate arbitrary protocol sets running at lane speeds anywhere from 1 to more than 40 Gigabits/s. The baseline configuration includes the ability to instantiate one or more channels of *Ethernet*, each channel operating at three selectable speeds of 1, 2.5 and 10 Gigabits/s. The present generation ("Gen-I") RCE provides support for three different computational models:

— A 450 MHz *PowerPC* processor configured with 128 or 512 MB of RLDRAM-II as well as 128 MB of configuration memory. Standard GNU tools are available for cross-development.

— Up to 192 Multiple-And-Accumulate (MAC) units. Each MAC is capable of one cycle, 18 *x* 18 fixed-point multiplication summed into a 48-bit accumulator. MACs may be operated either independently or cascaded together.

— Generic combinatoric logic and high-speed block RAM.

---

[112] R. Bartoldus et al, *High Bandwidth DAQ R&D for ATLAS Upgrade*, Version V1-3-0, 11 Feburary 2011.

An application is free to distribute their specific computation over these three mechanisms in any appropriate fashion. Independent of the mechanism used, all three mechanisms have access to data transmitted and received using the built-in serial I/O. In the case of the processor, a generic set of "DMA-like" engines are incorporated to transfer information between processor memory and serial I/O. These engines are optimized for low latency transfers and the underlying memory subsystem is able to sustain a continuous 8 Gigabytes/s of I/O. The processor is running under the control of a Real-Time kernel called *RTEMS*. RTEMS is an *Open Source* product, which contains, along with the kernel, POSIX standard interfaces as well as a full TCP/IP protocol stack.

In order to develop the RCE, the Gen-I RCE has been realized on an ATCA node (front) board. This board contains two RCEs. The RCE contains two dual-homed *Ethernet* interfaces. One is connected to the backplane's base interface and one to its fabric interface. The base interface operates at either 1 or 2.5 Gigabits/s while the fabric interface operates at 10 Gigabits/s. This board along with its corresponding RTM is shown in Figure 26. The RCE board. (The Media Slice controller and Terabyte of flash memory are only relevant to the PetaCache project.):
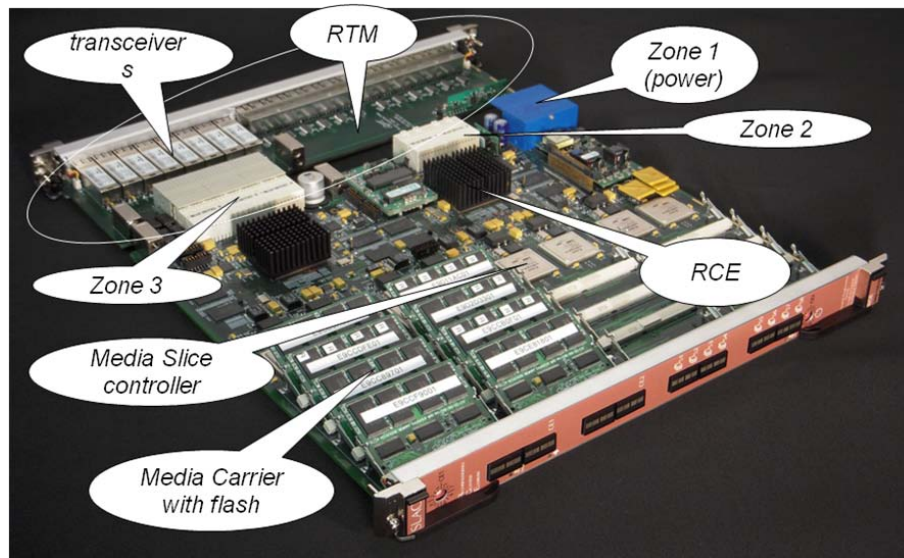
Figure 26. The RCE board. (The Media Slice controller and Terabyte of flash memory are only relevant to the PetaCache project.)

The RCEs are hidden behind their black heat sinks. The figure connectors used within the three ATCA zones are also called out. The connector used in Zone-3 (P3) is used to connect signals between the node board and its corresponding RTM. For this particular board the P3 connector carries the signals for eight serial links. Four of these links are connected to one RCE and the other four to the other RCE. The RTM simply contains eight optical transceivers (operating at 3.125 Gigabits/s), each converting a serial link from copper to fiber and fiber to copper. The fiber-optic links would typically be used to carry input data from front-end electronics systems. For example, in the case of ATLAS pixel readout applications, the RTM will contain TX/RX plug-ins for optical links connecting to the on-detector opto-boards for communicating with the pixel front-end electronics for clocks, configuration commands and DAQ data reception.

Readout noise Low-noise devices are measured in the number of electron, such as 2.8 e⁻.

ROIC Readout integrated circuit

ROS Read-Out System

Sensitive area 290.8 mm x 229.8 mm, 20 x 10 mm^2.

Sensor type or Image sensor type CMOS, CCD, monolithic CMOS, silicon PIN hybrid CMOS.

Time resolution microsecond

Window mode can be *Programmable*, *Full*, *Guide Window*.

5. X-ray detectors in the next decade

5.1 Development in different communities

Some of the future interests in X-ray detector technology can be summarized as follows.[113]

Application	X-ray Energy (keV)	Film Thickness (μm)	Area (cm^2)	Spatial Resolution (lp/mm)	Response Time (ms)
Crystallography	8 – 20	30 – 50	30 x 30	10	< 0.5
Mammography	20 – 30	100 – 150	20 x 25	15 – 20	< 0.1
Dental Imaging	50 – 70	70 – 120	2.5 x 3.5	7-10	NA
NDT	30 – 400	70 - >1000	>10 x 10	5 – 10	< 0.1
Astronomy	30 – 600	70 - >2000	30 x 30	4 – 5	<0.05

Note: NDT stands for non-destructive testing.

Besides medical and commercial interests, additional interest on hard X-rays above 10 keV comes from synchrotron/XFEL, and high-energy particle physics community.

XFEL's and Synchrotrons

In the near future, XFEL's and synchtrontron's main focus will still be on photons with < 30 KeV energy. For 50 keV photons in MPDH, alternative materials to silicon have to be used for higher efficiencies (above 50%) and compact pixel/voxel size (for better spatial resolution). At 50 KeV, roughly 5x as many electrons/photon are generated as at 10 keV, and so the detector dynamic range

---

[113] V. V. Nagarkar, *Structured CsI(Tl) Scintillators for X-ray Imaging Applications,* Radiation Monitoring Devices, Inc., 44 Hunt St., Watertown, MA 02172, USA

may be reduced. It normally takes five to ten years to develop a new technology based on the past experience from the community- if it can be done at all. The European XFEL is funding three institutions to build gated 200ns detectors to the tune of $15M total (Max Planck, DESY, Rutherford).

Astronomy

Property	XMM-Newton	eROSITA	XEUS
Status	Operating	Prototyping	Research
Type	Full frame pnCCD	Frame store pnCCD	Frame store pnCCD or Active Pixel Sensor (DEPFET APS)
Format	400×384	384×384	1024×1024
Pixel size (μm^2)	150×150	75×75	50×50 or 75×75
Readout noise	5 electrons	2 electrons	2 electrons
Sensitive thickness (μm)	295	450	450
Frame rate (fr. s^{-1})	14	20–1 000	200–1 000
Output nodes per CCD	12	3	32
FWHM(Mn–K_α) (eV)	150	130	125
FWHM(O–K) (eV)	90	60	50
Energy range (keV)	0.3–15	0.2–20	0.1–20

Figure 27. Properties of CCD detectors used in current and future X-ray missions in astronomy.[51]

NeXT is a Japanese satellite that can image X-ray energies up to 80 keV.[114]

High-energy particle Physics

Large-area picosecond photo-detectors project[115] is undertaken by a group from The University of Chicago, Argonne, Fermilab and UC Berkeley. The consortium is interested in the development of large-area systems to measure the time-of-arrival of relativistic particles with (ultimately) 1 pico-second resolution, and for signals typical of Positron-Emission Tomography (PET), a resolution of 30 pico-seconds (sigma on one channel). These are respectively a factor of 100 and 20 better than the present state-of-the-art. The development is divided into in a number of intellectually challenging areas: three-dimensional modeling of photo-optical devices, the design and construction of fast, economical, low-power electronics, the `end-to-end' (i.e. complete) simulation of large systems, real-time image processing and reconstruction, and the optimization of large detector and analysis systems for medical imaging. In each of these areas there is immense room for creative and innovative thinking, as the underlying technologies have moved faster than the applications. The group combines expertise from High Energy Physics, Radiology, and Electrical Engineering.

---

[114] S. Takagi, et al., Nucl. Instr. and Meth. A (2005)
[115] http://psec.uchicago.edu/; http://psec.uchicago.edu/workshops/fast_timing_conf_2011;

5.2 Basic research activities

At smaller scales, it is impossible to predict the outcome of the basic research efforts that can revolutionize X-ray detection. Therefore, the following discussions are organized into segments that match the building blocks of an X-ray detector as we know today.

Materials discovery for X-ray capture and conversion

Scintillator development at Caltech.[116] Over the last two decades, Dr. Ren-Yuan Zhu and his colleagues have been involved in the successful development of scintillating crystals for precision crystal electromagnetic calorimeter in high energy physics, such as the L3 BGO, BaBar CsI(Tl) and CMS PWO. In the last decade, several Advanced Detector Research awards were received from DOE for the development of PWO and LSO/LYSO crystals. In 2009, Ren-Yuan Zhu established a program for crystal development in the Caltech HEP. The main goal of this program is to develop novel detector concepts based upon crystal scintillators for future HEP experiments, such as LSO/LYSO for precision crystal electromagnetic calorimeter and cost-effective crystal scintillators for the homogeneous hadronic calorimeter detector concept.

CrystalSub-nanosec (pico-second) fluorescent material development. Cerenkov detectors using nanomaterials. A Cerenkov detector satisfies the condition

$$\beta n > 1 \qquad\qquad (25)$$

It is possible to develop photonic materials that have large n so that β, in particular electron β_e can be reduced significant, even to hard X-ray regime. For 40 keV electrons, $\beta_e = 0.37$, therefore n≥ 2.7. For 10 keV electrons, $\beta_e = 0.19$, therefore n ≥ 5.1.

Electro-optical crystals such as $LiNbO_3$. It is well known that the response time of the polarizability of optical crystals is in the femtosecond regime. Contact Thomas Tsang, BNL.

New photocathode, photodiode development. Fast MSM photodiode. Over the past decade, studies have indicated that it is possible to utilize the ultrafast (picosecond) response time of a photoconductor to detect and time resolve the rapid variations of light from a pulsed source, the intensity of which usually varies over a wide range. Photo-conducting radiation detectors is simple. Some of the examples include semi-insulating silicon, gallium-arsenide, and indium-phosphide. The main limitations of these materials are their low radiation resistance, low level of maximum DC bias and thermal runaway effects at high intensity. In order to circumvent these problems, it is necessary to consider semiconducting materials with wider bandgaps and large dielectric strengths that can support higher voltages. One of such a candidates is diamond and diamond thin films.

---

[116] http://www.hep.caltech.edu/~zhu/.

Nanoparticle usage to lower the pair-production energy threshold in gas, semconductors and scintillating detectors. Nano-wire chambers in solids. metallic Single-Walled Carbon Nanotubes (SWNT) detectors, SWNT, with diameter of typically 0.6-1.5 nm, are being developed into detectors. Led by Sigfrid Yngvesson, University of Massachusetts, Amherst and Eric Polizzi.

Superconducting nanowire single-photon detectors (SNSPD) are based on a superconducting wire cooled well below the superconducting transition temperature and biased with a dc current that is close to but less than the superconducting critical current. The SNSPD is typically made from≈ 5 nm thick niobium nitride films which are patterned as narrow nanowires (with a typical width of 100 nm). Absorption of a photon breaks Cooper pairs and reduces the critical current below the bias current. A small non-superconducting section across the width of the nanowire is formed.[117] This resistive non-superconducting section then leads to a detectable voltage pulse of a duration of about 1 nanosecond. The main advantages of this type of photon detector are its high speed (a maximal count rate of 2 GHz makes them the fastest available) and its low dark count rate. The main disadvantage is the lack of intrinsic energy resolution.

Molecular detectors. A new method to detect changes in molecular structures in a time of 0.1 ps (pico second), can potentially be used as powerful tools for detectors. Molecules that suddenly transform into new structures when stimulated by photons or electrons play key roles in many chemical and biological processes. Recently, chemists have discovered that adding transition metals such as copper to photo-responsive organic ligands produces materials with high solar conversion efficiencies, owing to the metal's ready supply of light-activated electrons. But despite the interest in these substances for opto-electronic devices, their inner workings remain mostly inscrutable because the charge-transfer dynamics happen too quickly for detection by typical instruments.

Tahei Tahara and colleagues from the RIKEN Advanced Science Institute, Wako, have spearheaded development of ultrafast laser spectroscopy that can capture these high-speed reactions by taking 'snapshots' of photochemical transformations with fs (10^{-15} s) accuracy. Now, an unprecedented finding by the research team—a ps (10^{-12} s) time delay during a theoretically instantaneous distortion—is set to overturn current thinking about light-driven rearrangements in transition metal complexes.

Copper dimethylphenanthroline is a compound containing two propeller-shaped wings, made out of thin aromatic sheets. Chemists regularly use it to explore photo-induced structural changes. In its unexcited state, the complex's wings are

---

[117] Semenov, A. D.; Gol'Tsman, Gregory N.; Korneev, Alexander A,. Quantum detection by current carrying superconducting film. *Physica C* **351** (2001) 349–356; Gol'tsman, G. N.; Okunev, O.; Chulkova, G.; Lipatov, A.; Semenov, A.; Smirnov, K.; Voronov, B.; Dzardanov, A. et al. "Picosecond superconducting single-photon optical detector". *Applied Physics Letters* **79** (2001) 705–707.

oriented perpendicular to each other. But when illuminated at a specific wavelength, the copper ion absorbs a photon and transfers an electron to the sheets—an action that flattens the structure by disrupting critical copper—phenanthroline bonds.

Quantum recording and readout devices

Spintronics devices is one form of quantum recording device. Energy does not have to be the only form of information carrier. In conventional detection paradigm, an energetic charged particle (electron, for example) is detected through a charge multiplication process [e, E] $\rightarrow$ [ne, f(E')]. Information buried in spin, which makes an electron act like a tiny bar magnet, is normally neglected. When the secondary electrons are in a spin polarized state (n↑ >> n↓), the change of the spin polarization provides additional information that may become useful for particle detection, through [e, E] $\rightarrow$ [ne, f(E'), mS]; Compared with the charge and kinetic energy of an electron, spin is unique in its own way through combining the `nice' features from both the quantum and classical world. Spin is quantized, like the charge, but spin can change, like energy. The kinetic energy change, except in a quantum well, is usually continuous, but the change of spin is discrete and only one of the two states is possible. Therefore, spintronic devices, which exploit either solely the spin properties or the combined charge and spin properties of electrons simultaneously, can be used as `spintronic detectors' for charged particles. Since the magnetic moment of an electron is about two thousand times that of a proton, detectors based on electronic spin may find their uses first. In principle, however, nuclear spin is just as attractive for detectors as electronic spin, and nuclear spin devices may be more sensitive than electronic devices.

Potential application of quantum bits in large data storge for X-ray detectors (to be completed).

Picosecond-gating for large areas

Optotronics

Attosecond science

Picosecond amplifiers

Fast amplifiers, if possible, require large input power.

5.3. Single-frame ps-resolution X-ray camera

6. Electron radiography and imaging

Using electrons for 2D and 3D imaging comes in a variety of forms. Well-known examples include scanning electron microscopy, transmission electron

microscopy, scanning tunneling electron microscopy, and more recently atomic force microscopy. Electron tomography is an extension of transmission electron technique to obtain 3D structures of objects. Images can be produced directly by the primary beam, or secondary particles such as Auger electrons, characteristic X-rays and visible light, specimen current.

Scanning techniques are too slow to measure fast (ns) and ultrafast (ps and sub-ps) events in MPDH. Ultrafast electron microscopy for materials science, biology and chemistry is currently a new frontier.[118] The main challenges lie in generating ps and sub-ps electron bunches with a sufficient intensity. The usual electron techniques also employ low energy beams that can not transmit through thick MPDH samples. Higher energy e-beams means apparatus bigger than the table-top scale, which limits the electron beam energies to tens of MeV.[119] RF-based MeV electron sources have been around longer than the table-top-laser based sources. Twenty GeV e-beam radiography is convenient for MPDH since such a beam is already available through XFEL. It is expected that a single electron bunch cam deliver 10^9 electrons with a pulse length of about 0.2 ps.

The mean free path of electronic transmission is not as well defined as X-rays or heavy ions such as protons due to energy straggling. High-resolution transmission electron microscopes, although capable of extraordinary resolution, are limited by multiple electron scattering to specimens thinner than 0.5–1μm.[120] Independent of particle usage, be it uncharged radiation, such as X-rays and neutrons, or charged particles, such as electrons, protons, or muons and others, the qualities of all the radiography and imaging are determined by a common set of parameters, including the source size (both the physical size and emittance), incidental and transmitted intensity, time-structure of the incidental beam, imaging optics, scattered background, detector blur and efficiency.[121]

Compared with X-ray imaging, some of the key differences using electrons for imaging are (to be completed).

Most exsiting detectors for electrons and ions are essentially the same as X-ray detectors. For low energy electrons, the dead-layer, which normally is a thin layer covering the detector, needs to be minimized. Dead-layer is not an issue for high energy electrons.

---

[118] W. E. King, G. H. Campbell, A. Frank et al. *Ultrafast electron microscopy in materials science, biology and chemistry,* J. Appl. Phys. **97** (2005) 111101.

[119] S. D. Mangles, B. R. Walton Z. Najmudin et al., *Table-top laser-plasma acceleration as an electron radiography source,* Laser and Particle Beams **24**, (2006) 185; F. Merrill et al., *Electron radiography,* NIM B **261**, (2007) 382.

[120] Grimm, R., Singh, H., Rachel, R., Typke, D., Zillig, W. & Baumeister, W. (1998) *Biophys. J.* **74,** 1031–1042; Jacobsen, C., Medenwaldt, R. & Williams, S. (1998) in *X-Ray Microscopy and Spectromicroscopy*, eds. Thieme, J., Schmahl, G., Umbach, E. & Rudolph, D. (Springer, Berlin), pp. II93–II102; J. Plitzko, A. Frangakis, S. Nickell, F. Forster, A. Gross, W. Baumeister, Trends Biotechnol. 20 (Suppl. (8)) (2002) S40–S44.

[121] N. S. P. King et al., *An 800-MeV proton radiography facility for dynamic experiment,* NIMA **424** (1999) 84.

7. Proton radiography

Although the performance of proton radiography could be greatly improved by using a proton beam in the 20 GeV or greater range,[122] this option is not being considered for MPDH at the moment. The functional requirements for MPDH are based on experiments using the same energy of 800 MeV protons as the existing LINAC. In order to accommodate the dynamic experimental needs of MPDH, a single proton bunch charge increase by a factor of 10 is proposed for better image statistics, that is, an increase from the existing value of 0.075 nC of charge, or 5×10^8 protons to 5×10^9 per bunch.[123] In addition, since single charge bunch spreads out to only about 200 ps, individual image frame could contain a motion blur of 200 nm for a shock front propagating at 10 km/s, which is much smaller than other sources of resolution limit, such as lens aberration, and detector resolution. The frame separation time is currently limited by a scintillator decay time of 42 ns;

Many dynamic radiography experiments at LANL require multiple high-resolution frames, in addition to short (< 150 ns) exposure and inter-frame times combined with high dynamic range. Since it is difficult to meet those demands with the present 3-frame hybrid CMOS cameras, or other current commercial CCD or monolithic CMOS cameras,[124] we have undertaken a new project to develop a new fast multi-frame imager. The new imager has a hybrid architecture, and it operates in a burst mode. It consists of a 1.2Mpx high-QE of > 85% (380nm-to-900nm), 100 μm thick silicon sensor, which is bump bonded to a pixelated CMOS read-out integrated chip (ROIC). As of November 2011 the CMOS ROIC chip design has been completed. It will be implemented in a 180 nm CMOS process. The expected performance parameters of the new 10-frame and the existing 3-frame imagers are compared in Table 1. To speed-up the data read-out each column of the imager is equipped with fast single-ramp 13-bit ADC's. The effective 12-bit dynamic range is maintained down to ~100 ns shutter time. The large size of the ROIC chip (47×49 mm^2) necessitates CMOS stitching in the wafer fabrication.

Table 1

Design Parameter	pRAD-1	pRAD-2

[122] C. L. Morris, J. W. Hopson and P. Goldstone, *Proton Radiography,* Los Alamos Science **30** (2006) 32.

[123] P. L. Walstrom, *Functional Requirements for Proton Radiography in MPDH* (Feb, 2011).

[124] S. Kleinfelder, S. W. Chiang, W. Huang, A. Shah and K. Kwiatkowski, *High-speed, high dynamic-range optical sensor arrays,* IEEE Trans. Nucl. Sci. **56** (2009) 1069; S. Kleinfelder, Y. Chen, and K. Kwiatkowski, *Multi-million frames/s sensor circuits for pulsed-source imaging,* IEEE Proc. *(2003); K.* Kwiatkowski, et al., *3-D stacked electronics assembly for high pixel-density array imaging detectors,* IEEE Proc. *(2003).*

	Imager	**2nd Gen Imager**
Minimum integration time (Global shutter)	150 ns	**50** ns
Nominal min. inter-frame time	350 ns	200 ns
Effective Dynamic Range	11.4 bits	12 bits
Read noise	100 e-	~ 37 e-
Imaging array size	720×720 px	1100×1100 px
Number of samples/ frames	3	**10**
Pixel pitch	26 μm	**40** μm
Sensor QE @ 415 nm	84%	>90%
Chip dimensions	21×22 mm^2	~**47×49** mm^2
Optical Fill-Factor	~100 %	~100 %
Saturation level/ Well depth	>200 ke-	~ 240 ke-

The camera can be used as a large imaging area (44mm×44mm) indirect x-ray detector via a lens-, or fiber-taper, coupling to a radiation-to-light converter (scintillator). In Laue diffraction experiments a thin single-crystal, or micro-columnar scintillator can be attached directly to the top of the pixelated sensor. At low x-ray energies (~10 keV) the 100 μm thick sensor can be used as a fast high-efficiency direct-detection imager.

8. Neutron imaging

Neutron imaging can complement X-ray imaging and charged particle radiography in many ways, mainly because neutrons interact with nucleus through nuclear force. Neutrons also interact with electrons magnetically, but the interaction is much weaker. In parallel with the other techniques, neutron

radiography and neutron phase contrast imaging[125] have been developed in the past. Neutron imaging is in general a slow process because of the time it takes to obtain an image with good contrast. A peak neutron flux from accelerator based sources is about 10^{15} neutrons/cm^2/s/Sr at the source location. Due to the dynamic and transient nature of the MPDH experiments, there will not be enough neutron intensity for imaging during a microsec or shorter time period.

The use of small angle neutron scattering (SANS) has been suggested for nuclear fuel rod imaging.[126] Detection of neutrons has been covered in depth in Knoll's book and references therein.[15]

9. Recommendations

At the present, no single detector system meets all the functional requirements of MPDH simultaneously. The needs for sub-ns frame rate and high efficiency in 50 keV X-ray detection are unique. Based on previous experience and ongoing activities from synchrotron and XFEL facilities, HEP and astronomy, a dedicated multi-year research and development effort on detectors would be required for MPDH.

The three challenges of MPDH detectors can be characterized as *the ps challenge, the GHz challenge, and the TB challenge*. In correspondence, three concerted focus areas of R&D are needed.

a.) High-efficiency (>50%) fast (~ a few hundred ps or less) X-ray detection at 50 keV and higher energies; X-ray detection and data recording needs finish before the next pulse arrives. The inter-pulse time is a few hundred ps, setting an upper limit in the duration of detection and recording.

b.) Sub-ns (~ 3 GHz or faster) frame rate X-ray cameras that can record a movie with up to 10,000 frames; and

c.) Detector architecture and engineering for optimal system performance, in particular for massive data storage and transmission.

For fast X-ray detection at high efficiency, MPDH can take advantage of the on-going pRad effort on a second-generation fast (50 ns) multi-frame imager. It is expected that at 10 keV X-ray energy, the existing 100 µm thick Si sensor can be used as a fast high-efficiency (above 50%) direct-detection imager. Later on, new generations of detectors based on high electron mobility and higher Z materials, such as InSb, can be developed. For example, absorption efficiency above 50%

[125] B. E. Allman et al., *Phase radiography with neutrons,* Nature **408** (2000) 158; B. E. Allman and K. A. Nugent, *Phase imaging with thermal neutrons,* Physica **B 385-386** (2006) 1395; D. L. Jacobson, B. E. Allman et al, *Thermal and cold neutron phase-contrast radiography,* Appl. Rad. Isot. **61** (2004) 547 – 550.
[126] R. Sheffield, P. Hosemann, S. A. Maloy, et al., *Nuclear Fuel and Structural Materials Research in Support of Fission/Fusion Reactors,* (2010).

for 50 keV photons can be readily achieved using a layer thickness of about 100 μm of InSb.

For the 3 GHz frame rate and the total number of frames up to 10, 000, the data rate is ~ 1.3 x 10^{19} byte of data per second = 3 x 10^9 (frame rate) x 10^6 (number of pixels) x 10^6 (dynamic range)/ 256 (8 bit per byte). In other words, within one μs or each event, ~ 10 TB is generated. For a 10 GHz (this the bit rate, the byte rate is 1/8) network (the state-of-the-art), it would require 8000 sec to transmit the data. Even for a future 1 THz network, it would require up to 80 sec for data transmission per event. Therefore, real-time data transmission is not realistic in the foreseeable future. On-board memories (in-pixel data storage) would be essentially to achieve both the high frame rate and to accommodate the large amount data. Detector architecture and engineering that integrate the detector array with recording array would be important. Significant involvements from micro-fabrication industry (ASIC technologies), academia, and possibly other DoE laboratories may be necessary to address the challenges.

It should be mentioned that the requirements in data acquisition, frame rate and data storage for each camera can be relaxed if multiple cameras are used. For example, if 5 cameras are used, then the data recording time can slow down by x5. The frame rate reduced by x5, and data storage reduced by x5. This would possibly require a x5 increase in source brightness.